Angewandte Chemie
Eine Zeitschrift der Gesellschaft Deutscher Chemiker

Supporting Information

Hierarchical Assembly of an Interlocked M_8L_{16} Container

Witold M. Bloch, Julian J. Holstein, Birger Dittrich, Wolf Hiller, and Guido H. Clever**

anie_201800490_sm_miscellaneous_information.pdf

Author Contributions

W.B. Corresponding author: Equal.

Contents

1. Experimental section

1.2. Materials and measurements

Unless otherwise stated, all chemicals were obtained from commercial sources and used as received. 3,6-Dibromo-9,10-dihexyloxyphenanthrene,[1] 9,10-dipropoxyphenanthrene and 9,10-dimethoxy-3,6-bis(4-pyridyl)phenanthrene[2] were prepared according to literature procedures. GPC purifications were performed on a JAI 9210-II NEXT GPC System with a JAIGEL HH-2/HH-1 column combination running with $CHCl_3$ (HPLC grade). Infrared spectra were collected on a Pelkin Elmer Spectrum Two spectrometer. Electrospray ionization (ESI) mass spectra were recorded on a Bruker Apex IV ESI-FTICR Mass Spectrometer with a dual electrospray ionization source. TEM measurements were performed on a Philips CM200 TEM high-resolution Transmission Electron Microscope equipped with an EDAX EDS system and Gatan 678 Image Filter and P/EELS, and Gatan 832 SC1000 CCD camera. DLS measurements were carried on a Malvern Zetasizer ZS equipped with a standard 633 nm laser. DLS samples were measured in acetonitrile in a 10 mm quartz cuvette. For Variable Temperature (VT) DLS measurements, the viscosities of CH_3CN at different temperatures were extracted from published data.[3] The peak size (d.nm) and polydispersity index (PDI) were determined from the autocorrelation functions using the Zetasizer software provided by the manufacturer.

1.3. Synthesis of ligands

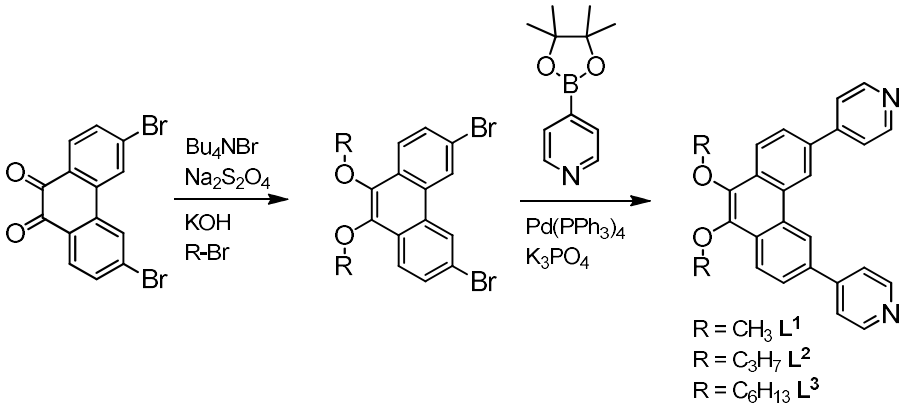

Scheme 1

1.3.1. Synthesis of 3,6-dibromo-9,10-dipropoxyphenanthrene

The synthesis of 3,6-dibromo-9,10-dipropoxyphenanthrene was carried out according to a procedure described by Mazal and co-workers.[4] 3,6-Dibromo-9,10-phenanthrenequinone (1.10 g, 3.00 mmol), Bu_4NBr (1.10 g, 3.41 mmol), and $Na_2S_2O_4$ (6.10 g, 35.0 mmol) were dissolved in aqueous THF (1:1, 44 mL) and stirred for 1 h. 1-Bromopropane (2.87 mL, 31.5 mmol) was added, followed by KOH (4.4 g, 78.4 mmol) in H_2O (22 mL). After stirring for 2 days at 25 °C, the reaction mixture was diluted with H_2O (75mL) and extracted with dichloromethane (3 × 30 mL). The extracts were dried over $MgSO_4$ and the solvent was removed under reduced pressure. The crude product was purified by column chromatography (CH_2Cl_2) and recrystallized from pentane to yield an off-white solid (0.92 g, 67%). Mp: 104.0 – 105.2 °C. ^{1}H NMR (500 MHz, $CDCl_3$) δ 8.65 (d, *J* = 1.8 Hz, 2H), 8.11 (d, *J* = 8.7 Hz, 2H), 7.71 (dd, *J* = 8.7, 1.8 Hz, 2H), 4.16 (t, *J* = 6.7 Hz, 4H), 1.91 (h, *J* = 7.3 Hz, 4H), 1.12 (t, *J* = 7.3 Hz, 6H). ^{13}C NMR (150 MHz, $CDCl_3$) δ 143.3, 130.6, 129.0, 128.9, 125.5, 124.4, 120.5, 75.4, 23.8, 10.9. ESI-MS ($C_{20}H_{20}O_2Br_2$) calc: 450.9858 [**M**+H]$^+$; found: 450.9796.

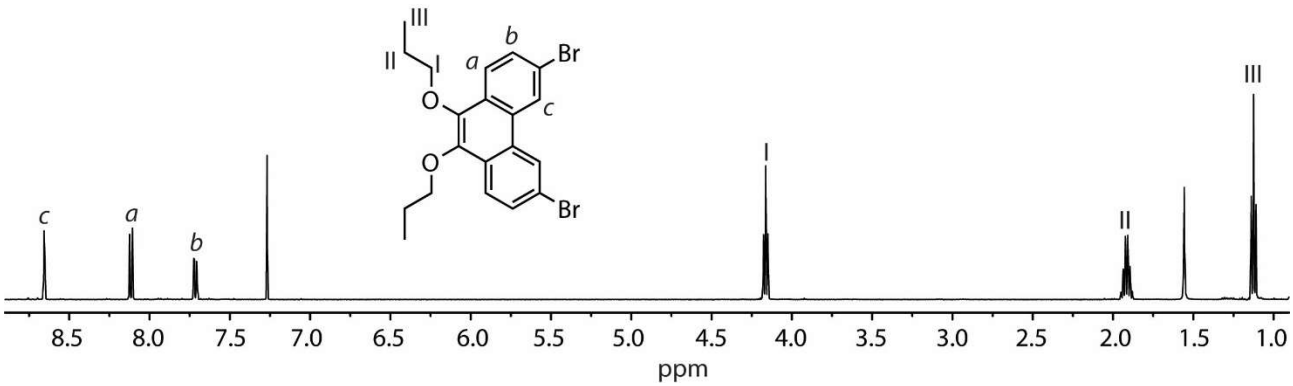

Figure S1. ^{1}H NMR spectrum (600 MHz/$CDCl_3$) of 3,6-dibromo-9,10-dipropoxyphenanthrene.

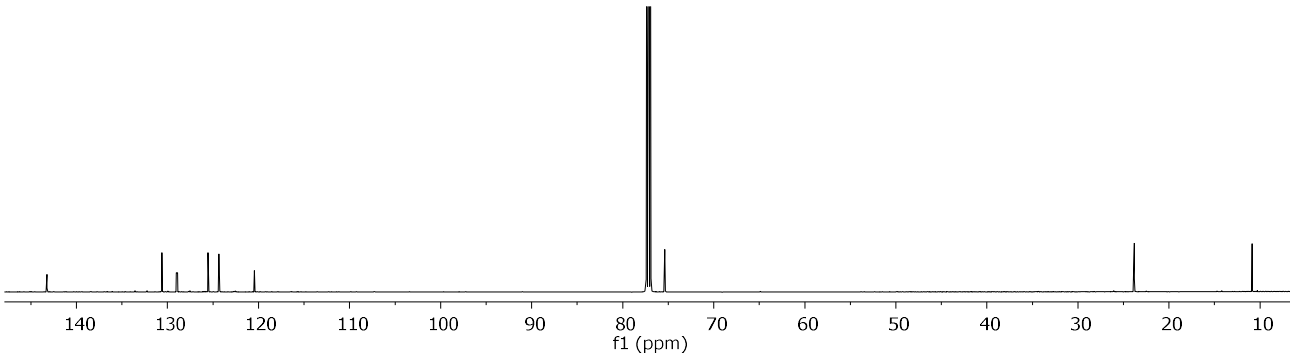

Figure S2. ^{13}C NMR spectrum (150 MHz/ $CDCl_3$) of 3,6-dibromo-9,10-dipropoxyphenanthrene.

*1.3.2. Synthesis of 9,10-dipropoxy-3,6-bis(4-pyridyl)phenanthrene (**L²**)*

3,6-Dibromo-9,10-dipropoxyphenanthrene (437 mg, 0.966 mmol), 4-pyridineboronic acid pinacol ester (594 mg, 2.90 mmol), K_3PO_4 (1.67, 7.9 mmol) and dioxane (32 mL) were combined in a schlenk vessel. Once the solvent was degassed (via freeze-thaw cycles), $Pd(PPh_3)_4$ (114 mg, 0.10 mmol) was added and the mixture was heated at 100 °C for 24 h. Once allowed to cool, water (40 mL) was added and the mixture was extracted with chloroform (4 × 15 mL). The combined organic layers were dried over $MgSO_4$ and the solvent was removed under reduced pressure. The residue was purified by column chromatography (CH_2Cl_2, 15:1 CH_2Cl_2/MeOH) and then further purified by GPC to yield the title compound as a white crystalline solid (185 mg, 42%). Mp: 160.6 – 162.7 °C; ν_{max} (neat, cm^{-1}): 2965 (w), 1592 (s), 1540 (w), 1440 (s), 1331 (m); ^1H NMR (600 MHz, CD_3CN) δ 9.18 (d, *J* = 1.8 Hz, 2H, H_c), 8.73 – 8.70 (m, 4H, H_e), 8.39 (d, *J* = 8.5 Hz, 2H, H_a), 8.03 (dd, *J* = 8.5, 1.8 Hz, 2H, H_b), 7.90 – 7.87 (m, 4H, H_d), 4.23 (t, *J* = 6.6 Hz, 4H, N-CH_2), 1.99 – 1.93 (m, 4H, CH_2), 1.15 (t, *J* = 7.4 Hz, 6H, CH_3); ^{13}C NMR (150 MHz, CD_3CN) δ 150.9, 148.3, 144.3, 136.0, 130.8, 129.4, 126.5, 123.9, 122.5, 122.4, 75.7, 24.0, 10.7. ESI-MS ($C_{36}H_{40}N_2O_2$) calc: 449.2224 [**L²**+H]$^+$; found: 449.2284.

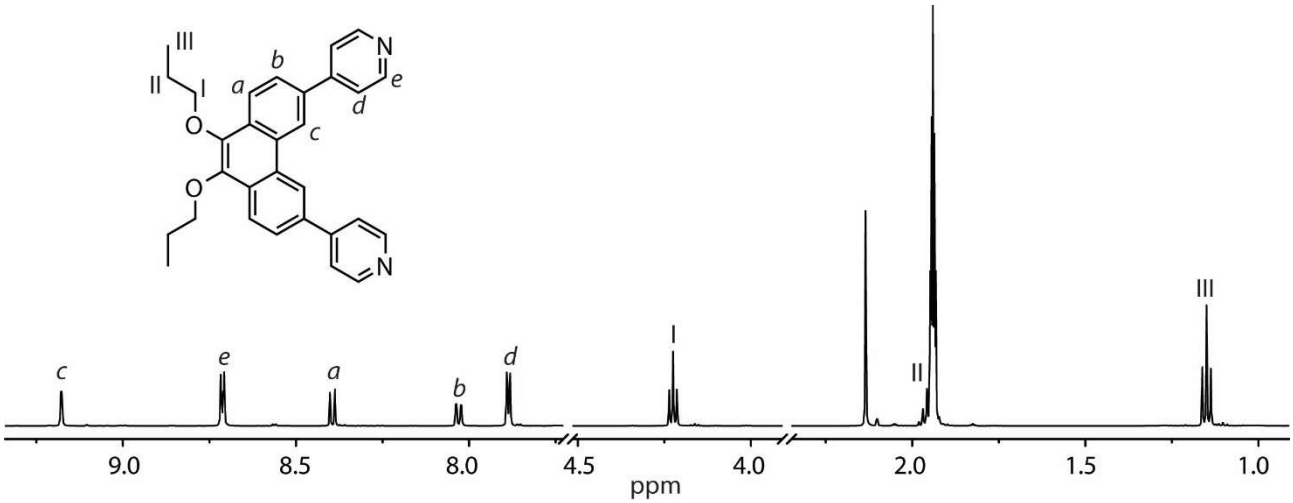

Figure S3. Partial ^1H NMR spectrum (600 MHz/CD_3CN) of **L²**.

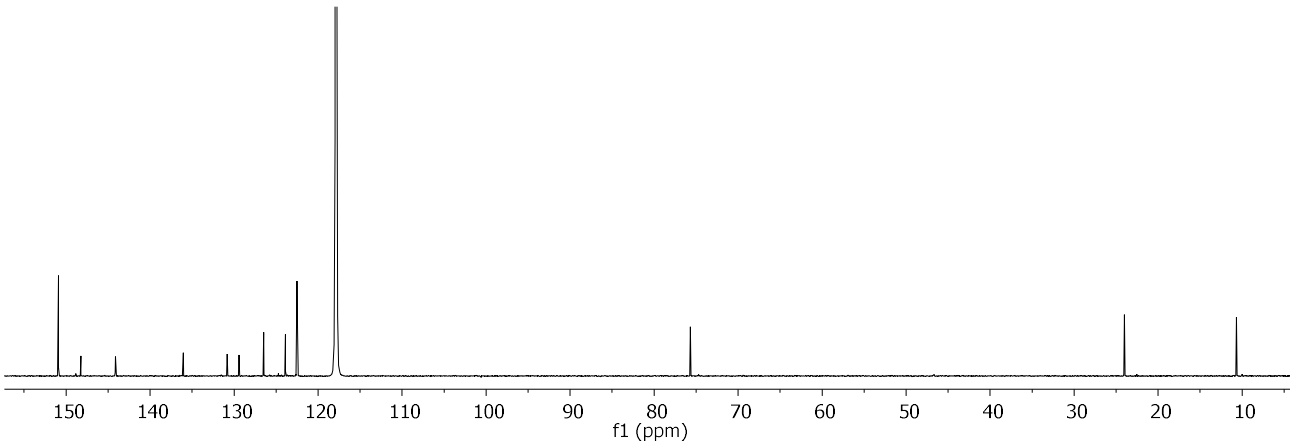

Figure S4. ^{13}C NMR spectrum (150 MHz/CD_3CN) of **L²**.

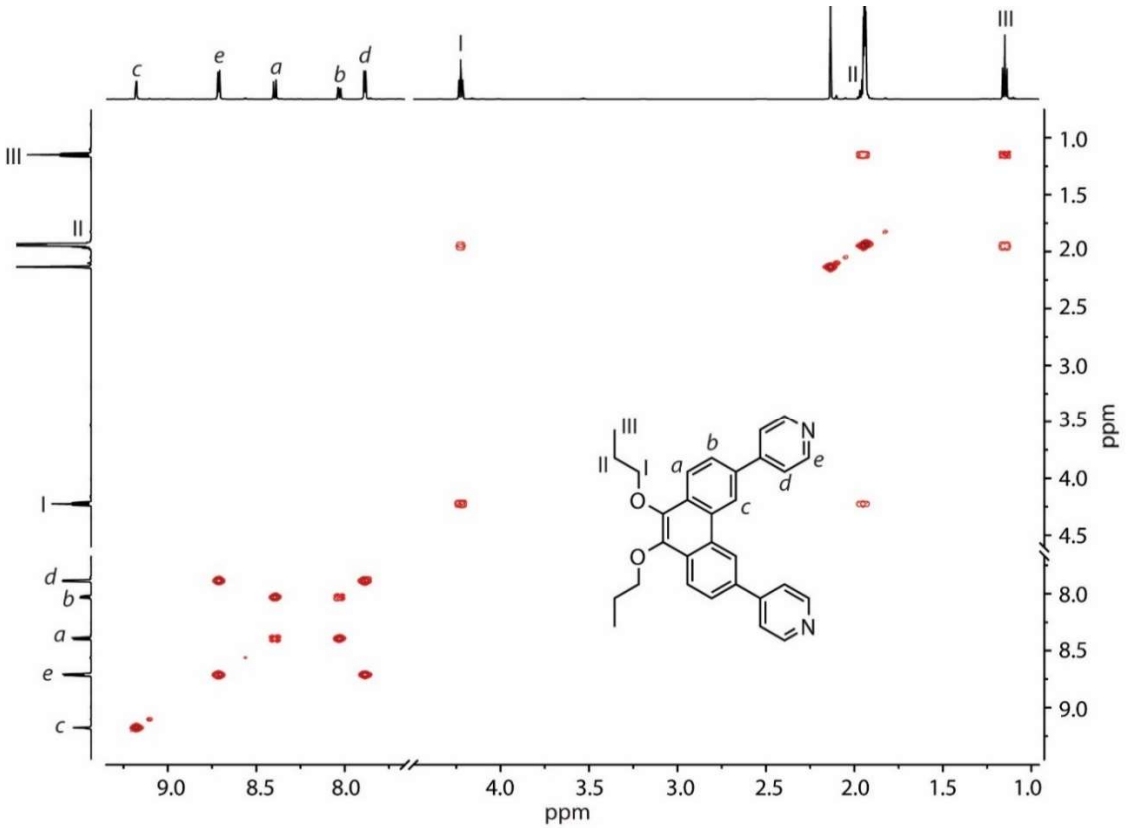

Figure S5. $^{1}H - {}^{1}H$ COSY spectrum (600 MHz/CD_3CN) of **L^2**.

*1.3.3. Synthesis of 9,10-dihexyloxy-3,6-bis(4-pyridyl)phenanthrene (**L^3**)*

3,6-Dibromo-9,10-dihexyloxyphenanthrene (300 mg, 0.557 mmol), 4-pyridineboronic acid pinacol ester (342 mg, 1.67 mmol), K_3PO_4 (0.97 g, 4.55 mmol) and dioxane (19 mL) were combined in a schlenk vessel. Once the solvent was degassed (via freeze-thaw cycles), $Pd(PPh_3)_4$ (65.4 mg, 0.056 mmol) was added and the mixture was heated at 100 °C for 24 h. Once allowed to cool, water (50 mL) was added and the mixture was extracted with chloroform (4 × 20 mL). The combined organic layers were dried over $MgSO_4$ and the solvent was removed under reduced pressure. The residue was purified by column chromatography ($CHCl_3$, 20:1 $CHCl_3$/MeOH) and then further purified by GPC to yield the title compound as an off-white solid (150.8 mg, 53 %). Mp: 112.6 – 113.4 °C; ν_{max} (neat, cm^{-1}): 2942 (m), 1594 (s), 1539 (w), 1439 (m), 1329 (m); ^{1}H NMR (500 MHz, CD_3CN) δ 9.18 (d, J = 1.8 Hz, 2H, H_c), 8.77 – 8.66 (m, 4H, H_e), 8.38 (d, J = 8.5 Hz, 2H, H_a), 8.03 (dd, J = 8.5, 1.8 Hz, 2H, H_b), 7.93 – 7.85 (m, 4H, H_d), 4.25 (t, J = 6.6 Hz, 4H, CH_2), 1.92 – 1.89 (m, 4H, CH_2), 1.67 – 1.55 (m, 4H, CH_2), 1.48 – 1.33 (m, 8H, 2 x CH_2), 0.98 – 0.89 (m, 6H, CH_3). ^{13}C NMR (150 MHz, CD_3CN) δ 151.3, 148.6, 144.6,136.4, 131.2, 129.8, 126.9, 124.3, 122.9, 122.8, 74.6, 32.4, 31.1, 26.6, 23.3, 14.3. ESI-MS ($C_{36}H_{40}N_2O_2$) calc: 533.3163 [**L^3**+H]$^+$; found: 533.3152.

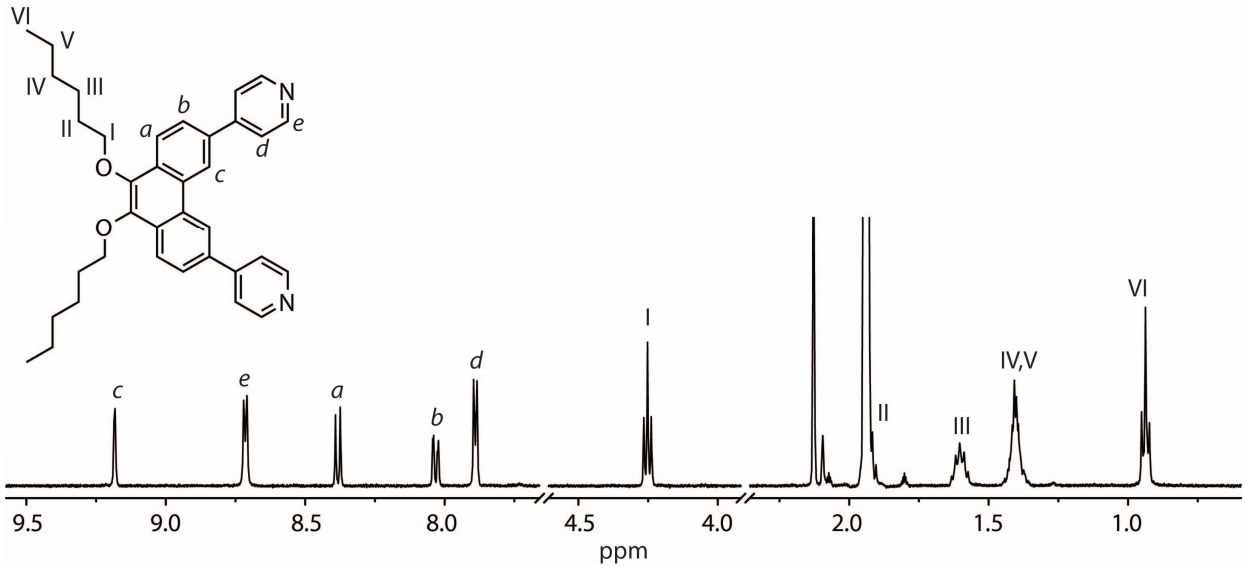

Figure S6. Partial ^{1}H NMR spectrum (500 MHz/CD_3CN) of **L^3**.

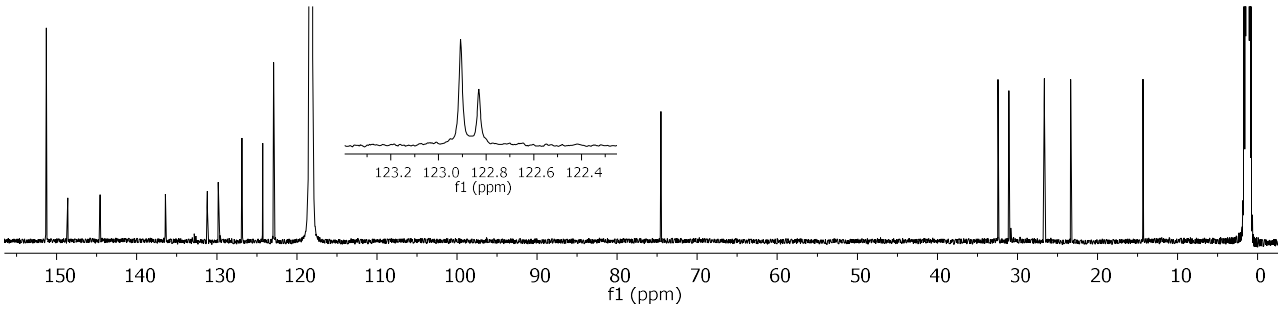

Figure S7. ^{13}C NMR spectrum (150 MHz/CD_3CN) of **L³**.

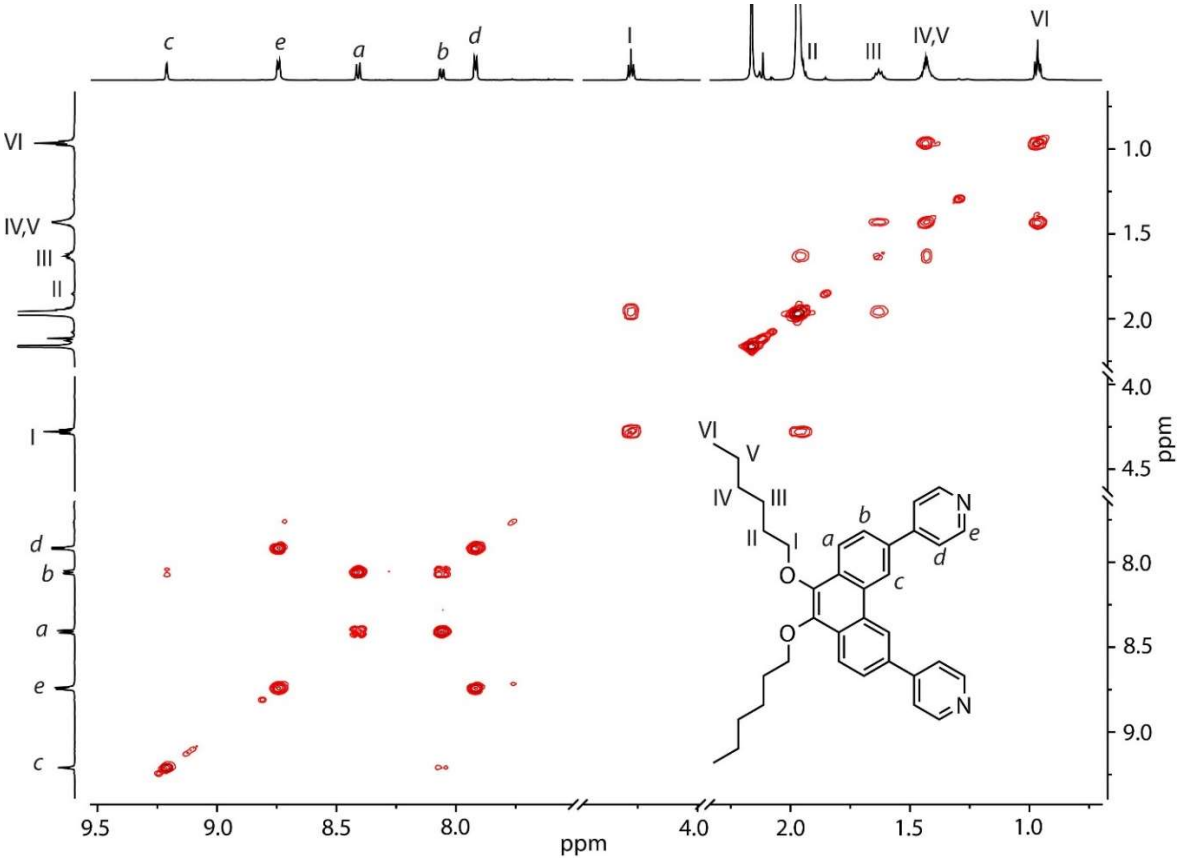

Figure S8. ^1H – ^1H COSY spectrum (600 MHz/CD_3CN) of **L**

1.4. Synthesis of metallosupramolecular assemblies

*1.4.1. Synthesis of a mixture of Pd_3**L¹**$_6$, Pd_4**L¹**$_8$ (D_{4h}), and Pd_4**L¹**$_8$ (D_{2d}) (**1a**, **1b** and **1c**)*

The synthesis of a mixture of **1a**, **1b**, and **1c** was carried out by heating a 2:1 mixture of **L¹** and $[Pd(CH_3CN)_4](BF_4)_2$ in CD_3CN for 2 h. Full experimental details including ^1H NMR and ESI-MS have been previously reported.[5]

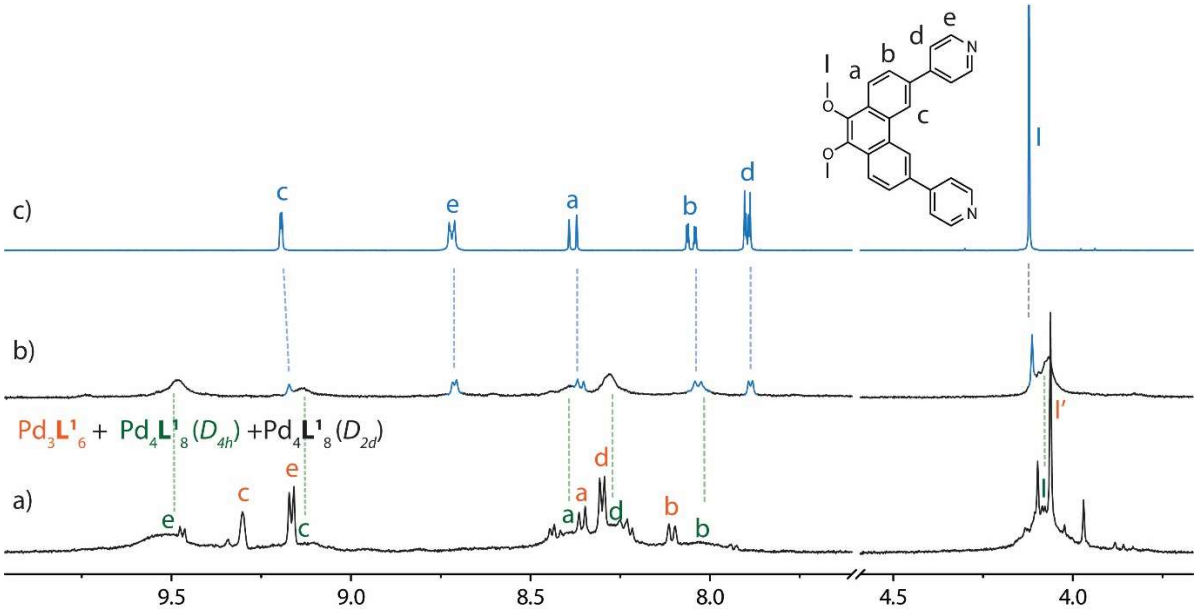

Figure S9. ^{1}H NMR spectra (500 MHz/CD_3CN) of: a) a mixture of **1a**, **1b** and **1c** (approximate ratio 1:2:0.2, respectively); b) a) heated for 24 h at 70 °C. The proton signals corresponding to **1b** (green, broad) remain whilst the signals corresponding to **1a** (orange) and **1c** disappear. Furthermore, signals corresponding to $\mathbf{L^1}$ (blue) appear suggesting that both **1a** and **1c** are not thermodynamically stable in CD_3CN; c) $\mathbf{L^1}$. Note: the change from a) to b) is accompanied by a precipitate which does not dissolve in common organic solvents, indicative of a polymeric side-product. Whilst the full proton spectrum of **1c** cannot be fully assigned in a) (due to peak overlap), the two methoxy proton signals at δ 4.10 and 3.97 are consistent with the D_{2d} symmetry of the tetrahedron **1c** (see section 5). The ESI-MS spectrum of this sample has been previously reported.[5]

*1.4.2. Synthesis of a $Pd_4\mathbf{L^1}_8$ (D_{4h}) **1b** from $Pd(NO_3)_2$ in DMSO*

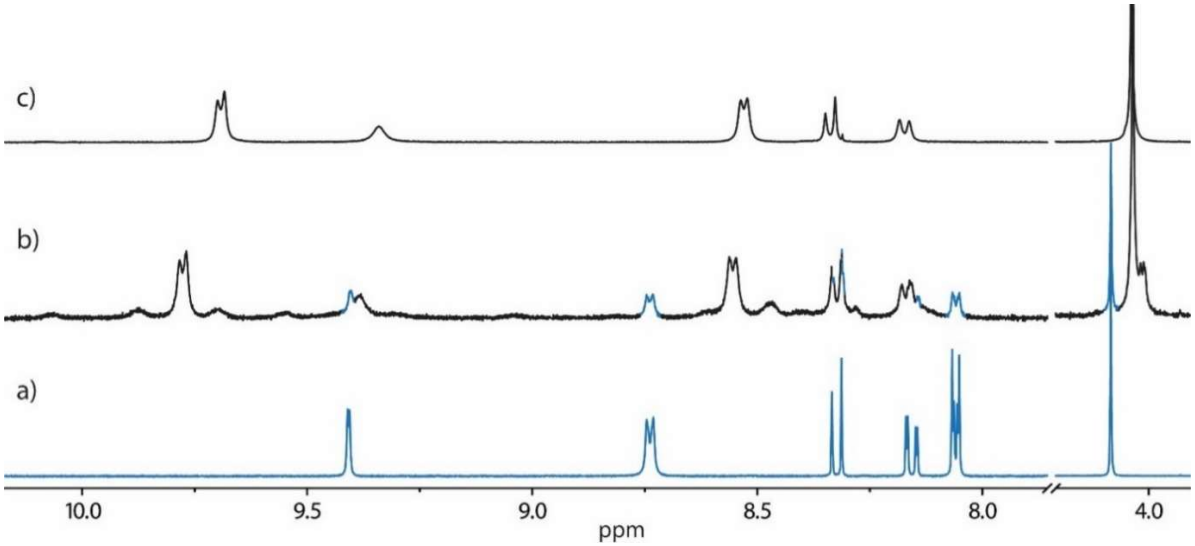

Figure S10. ^{1}H NMR spectra (500 MHz/DMSO) of: a) $\mathbf{L^1}$; b) a 2:1 mixture of $\mathbf{L^1}$ and $Pd(NO_3)_2$ (hydrate) in DMSO heated for 24 h at 70 °C. Proton signals corresponding to both **1b** and $\mathbf{L^1}$ (blue) are present; c) **1b**, prepared from $\mathbf{L^1}$ and $Pd(CH_3CN)_4](BF_4)_2$.[2] The small discrepancy in chemical shift of **1b** in b) and c) is due to the presence of NO_3^- counter-ions in b) and BF_4^- counter-ions in c).

*1.4.3. Synthesis of $[Pd_8\mathbf{L^1}_{16}]^{16+}$ (**2a**)*

A solution of palladium nitrate hydrate (368 µL, 15 mM/CD_3CN, 5.5 µmol) was combined with a solution of $\mathbf{L^1}$ (4.21 mg, 10.7 µmol) in CD_3CN (3463 µL) and heated at 70 °C for 24 h to afford $[Pd_8\mathbf{L^1}_{16}]^{16+}$. ^{1}H NMR (700 MHz, CD_3CN) δ 10.72 (d, J = 6.1 Hz, 16H), 10.16 (d, J = 6.2 Hz, 16H), 9.81 (d, J = 5.9 Hz, 16H), 9.59 (s, 8H), 9.42 (s, 8H), 9.19 (d, J = 6.0 Hz, 16H), 9.06 (s, 8H), 8.83 (d, J = 6.1 Hz, 16H), 8.68 (d, J = 6.0 Hz, 16H), 8.54 – 8.46 (m, 24H), 8.43 – 8.38 (m, 16H), 8.33 (d, J = 8.7 Hz, 8H), 8.09 (d, J = 8.8 Hz, 16H), 7.75 (d, J = 8.5 Hz, 8H), 7.26 (d, J = 8.6 Hz, 8H), 6.65 (d, J = 8.7 Hz, 8H), 4.09 (s, 24H), 4.07 (s, 24H), 3.87 (s, 24H), 3.44 (s, 24H). ^{13}C NMR (150 MHz, CD_3CN/DMSO 2:1): δ 152.4, 152.1, 152.0, 151.5, 151.3, 150.8, 145.3, 145.2, 144.8, 143.8, 135.0, 133.9, 132.6, 132.3, 131.5, 131.2, 130.2, 129.8, 129.3, 129.2, 128.8, 128.2, 127.5, 127.0, 126.8, 126.3, 126.0, 124.9, 124.8, 124.2, 124.2, 124.1, 123.9, 123.8, 123.50, 122.7, 122.4, 122.0, 61.39, 61.37, 61.1, 60.6. ESI HR-MS ($C_{416}H_{320}N_{32}O_{32}Pd_8$) calc: 840.5108 [**2a**+7NO_3]$^{9+}$, 953.1982 [**2a**+8NO_3]$^{8+}$, 1098.2248 [**2a**+9NO_3]$^{7+}$, 1291.5939 [**2a**+10NO_3]$^{6+}$, 1562.3101 [**2a**+11NO_3]$^{5+}$, 1968.3849 [**2a**+12NO_3]$^{4+}$; found: 840.5089 [**2a**+7NO_3]$^{9+}$, 953.1991 [**2a**+8NO_3]$^{8+}$, 1098.2248 [**2a**+9NO_3]$^{7+}$, 1291.5984 [**2a**+10NO_3]$^{6+}$, 1562.3111 [**2a**+11NO_3]$^{5+}$, 1968.3801 [**2a**+12NO_3]$^{4+}$.

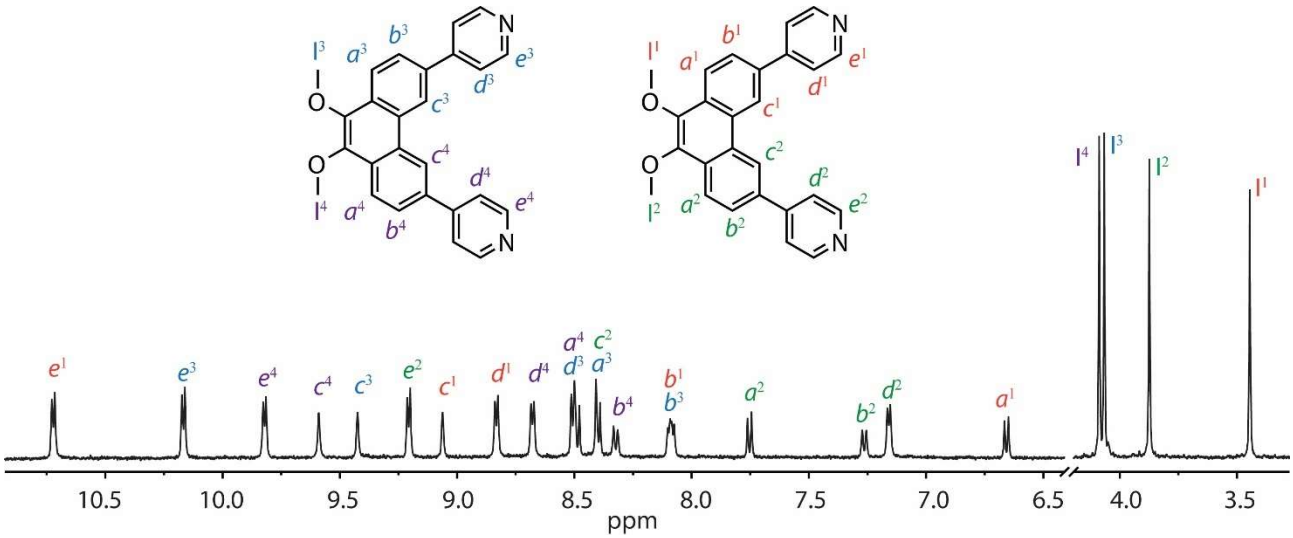

Figure S11. Partial ^{1}H NMR spectrum (500 MHz/CD_3CN) of **2a**.

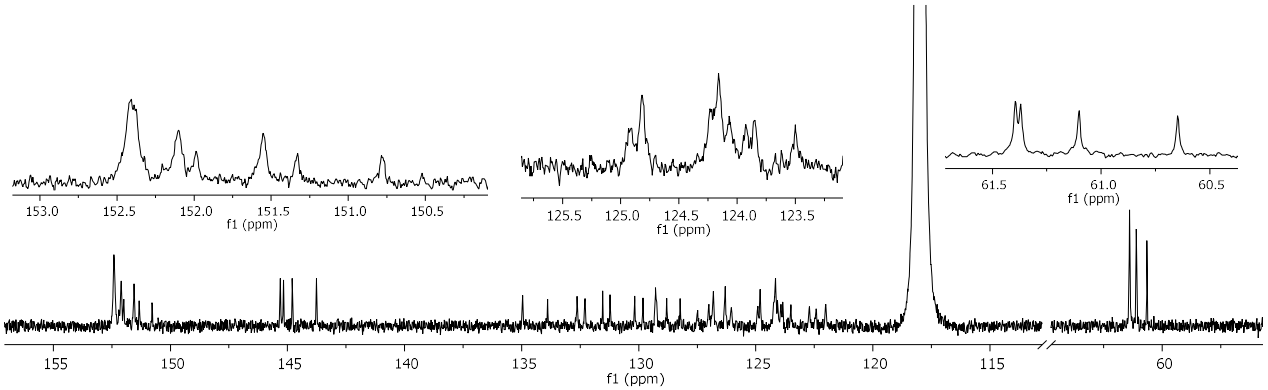

Figure S12. Partial ^{13}C NMR spectrum (150 MHz/ CD_3CN/DMSO 2:1) of **2a** showing expansions of the regions containing overlapping signals. Of the 52 expected ^{13}C signals, only 44 could be clearly identified.

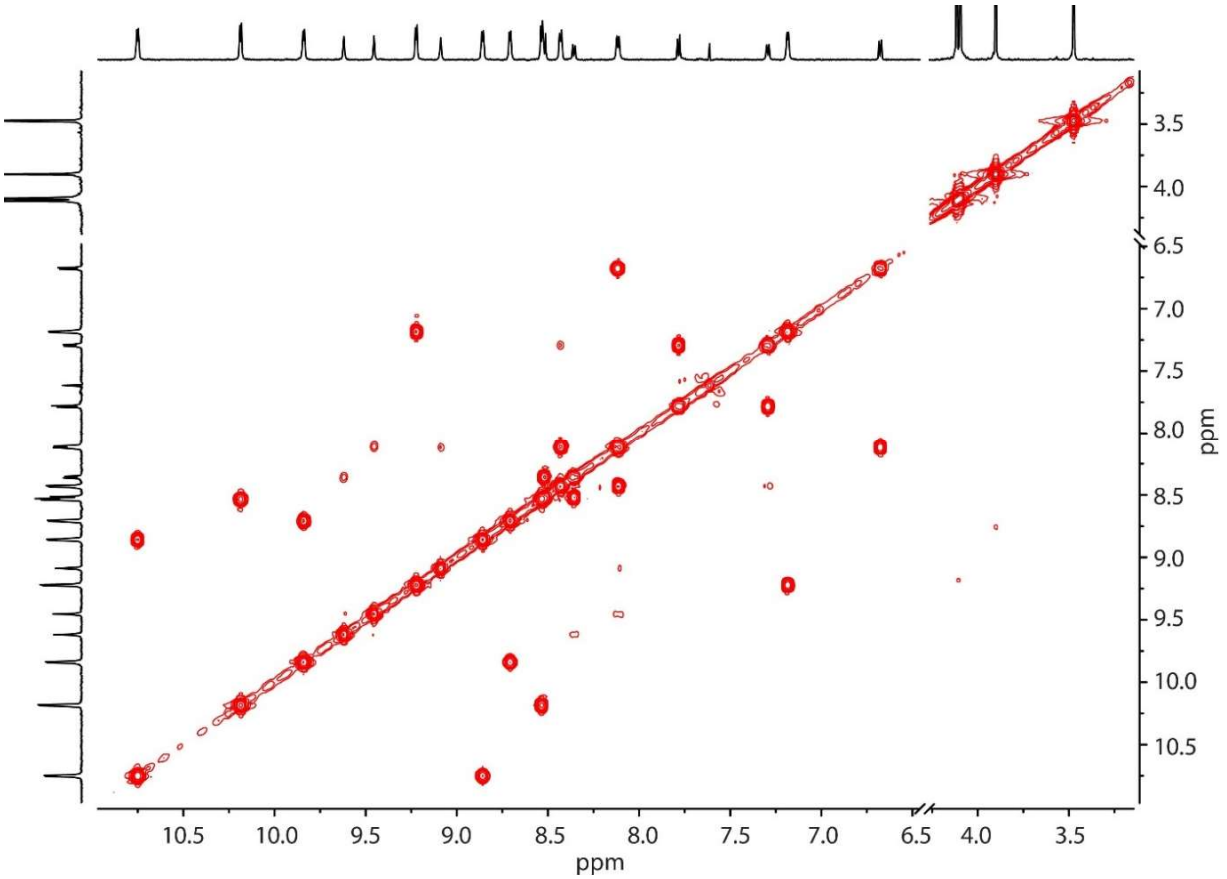

Figure S13. ^{1}H – ^{1}H COSY spectrum (600 MHz/CD3CN) of **2a**.

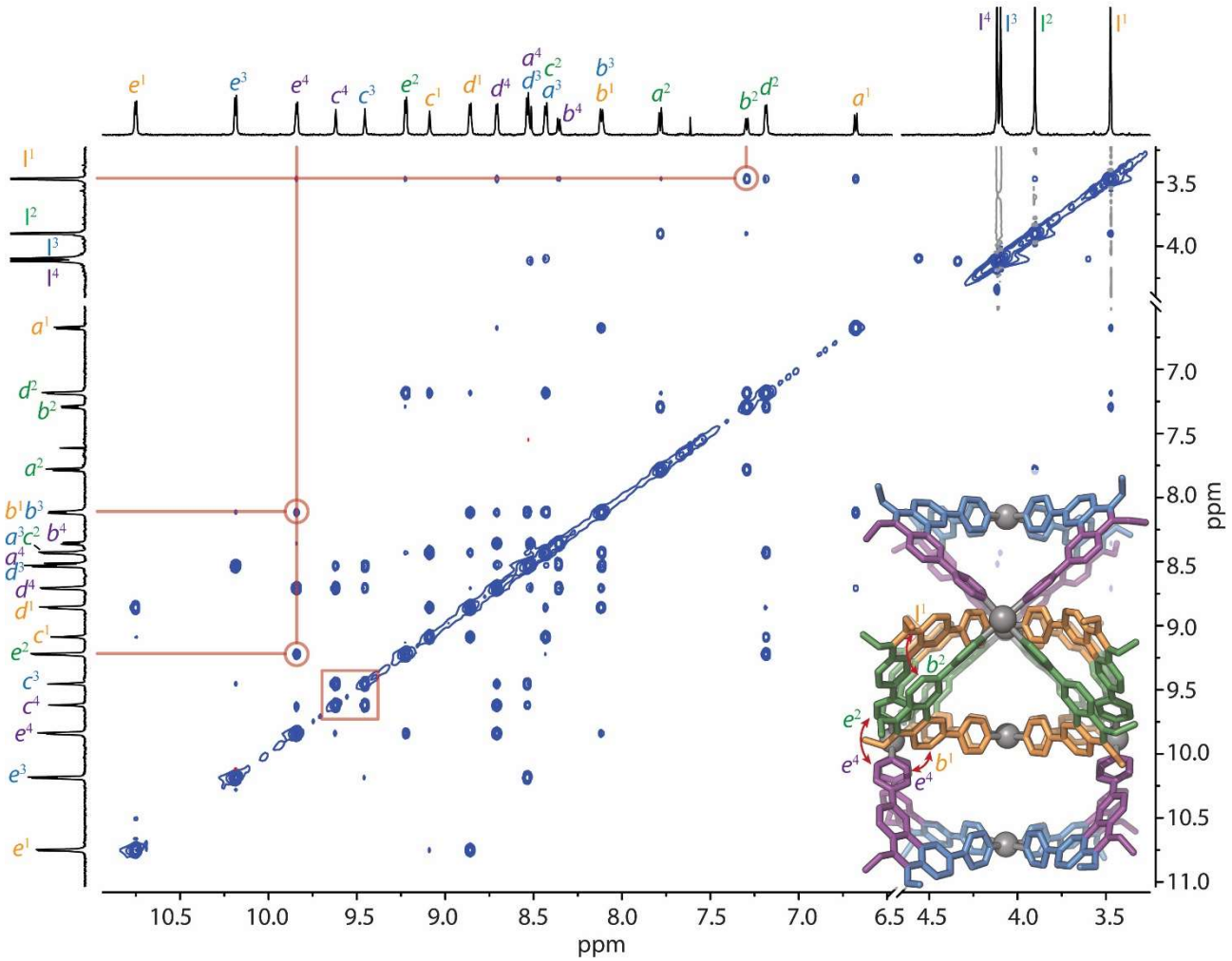

Figure S14. ^{1}H – ^{1}H NOESY spectrum (600 MHz/CD_3CN) of **2a** with important NOESY contacts highlighted in red. A symmetry-by-color model of **2a** based of the crystal structure of **2b** is shown in the inset. The loss in two-fold ligand symmetry can be clearly visualized as the result of interpenetration, with the central and peripheral ligands possessing distinct chemical environments. The X-ray structure is therefore fully consistent with fourfold-split ^{1}H NMR spectroscopic signature of the molecule.

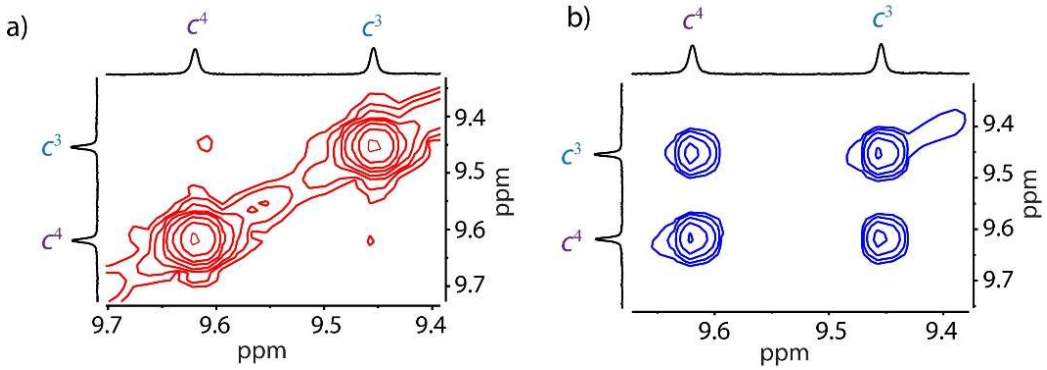

Figure S15. a) Partial ^{1}H – ^{1}H COSY spectrum (600 MHz/CD_3CN) of **2a** showing the weak ^{5}J coupling between adjacent H_c protons in one of the **L^{1}** ligands; b) Partial ^{1}H – ^{1}H NOESY spectrum (600 MHz/CD_3CN) of **2a** showing the cross peaks between adjacent H_c protons in one of the **L^{1}** ligands. This supports that, in **2a**, the ligands have lost their two-fold symmetry.

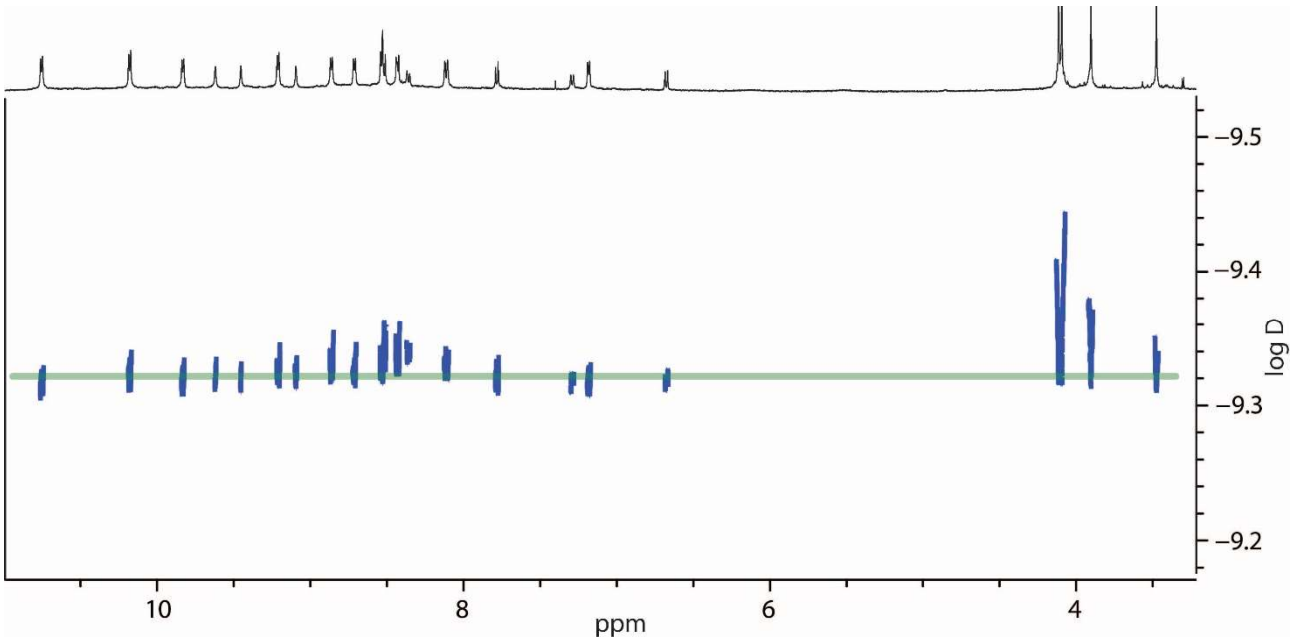

Figure S16. DOSY spectrum (600 MHz, CD_3CN, 25 °C) of **2a**. Diffusion coefficient: 4.79 x 10^{-10} m^2/s, hydrodynamic radius = 1.24 nm.

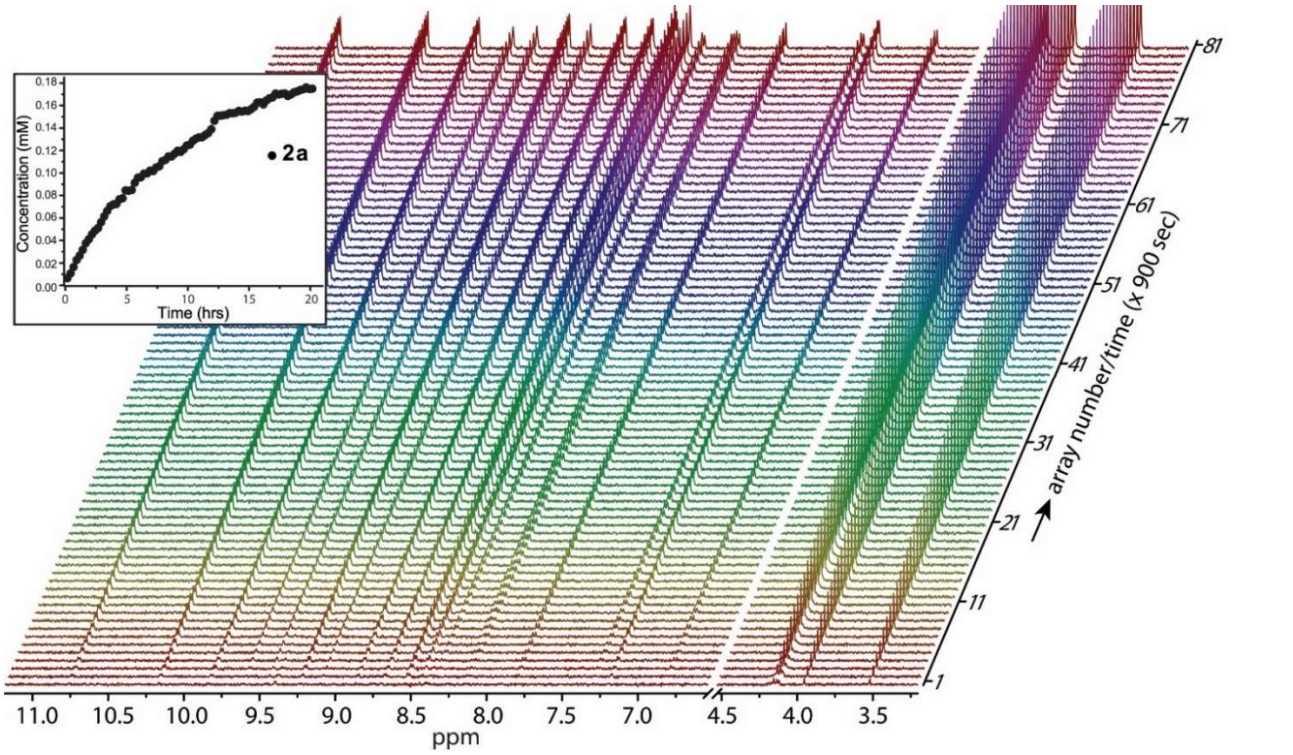

Figure S17. ^1H NMR (500 MHz, CD_3CN) array experiment carried out at 70°C showing the gradual formation of **2a**. The array experiment was carried out over 20.16 hrs in 15 min intervals. The inset shows the formation of **2a** based on a final concentration of 0.175 mM, calculated by comparing the integration of the aromatic signals to a standard solvent signal.

*1.4.4. Synthesis of $[Pd_8\mathbf{L^2}_{16}]^{16+}$ (**2b**)*

A solution of $Pd(NO_3)_2$ (387 µL, 15 mM/CD_3CN, 5.8 µmol) was combined with a solution of $\mathbf{L^2}$ (5.05 mg, 11.3 µmol) in CD_3CN (3634 µL) and heated at 70 °C for 24 h to afford $[Pd_8\mathbf{L^2}_{16}]^{16+}$. ^1H NMR (600 MHz, CD_3CN) δ 10.77 (d, J = 5.9 Hz, 16H), 10.15 (d, J = 6.0 Hz, 16H), 9.91 (s, 16H), 9.53 (s, 8H), 9.36 (s, 8H), 9.24 (d, J = 5.8 Hz, 16H), 9.11 (s, 8H), 8.88 (s, 16H), 8.67 (s, 16H), 8.54 – 8.44 (m, 24H), 8.41 (d, J = 8.8 Hz, 8H), 8.37 (s, 8H), 8.25 – 8.16 (m, 16H), 8.07 (d, J = 8.8 Hz, 8H), 7.74 (s, 8H), 7.16 (s, 8H), 7.08 (s, 16H), 6.89 (d, J = 8.6 Hz, 8H), 4.24 – 4.12 (m, 32H), 4.05 (s, 8H), 3.85 (s, 8H), 3.76 (s, 8H), 3.15 – 3.06 (m, 8H), 1.93 – 1.88 (m, 32H), 1.80 – 1.72 (m, 16H), 1.29 – 1.19 (m, 16H), 1.15 – 1.01 (m, 64H), 0.92 – 0.79 (m, 24H). ESI HR-MS ($C_{480}H_{448}N_{32}O_{32}Pd_8$) calc: 1065.5738 [**2b**+$8NO_3$]$^{8+}$, 1226.5112 [**2b**+$9NO_3$]$^{7+}$, 1441.2612 [**2b**+$10NO_3$]$^{6+}$, 1741.7110 [**2b**+$11NO_3$]$^{5+}$, 2193.1361 [**2b**+$12NO_3$]$^{4+}$; found: 1065.5897 [**2b**+$8NO_3$]$^{8+}$, 1226.5294 [**2b**+$9NO_3$]$^{7+}$, 1441.2823 [**2b**+$10NO_3$]$^{6+}$, 1741.9365 [**2b**+$11NO_3$]$^{5+}$, 2193.1646 [**2b**+$12NO_3$]$^{4+}$.

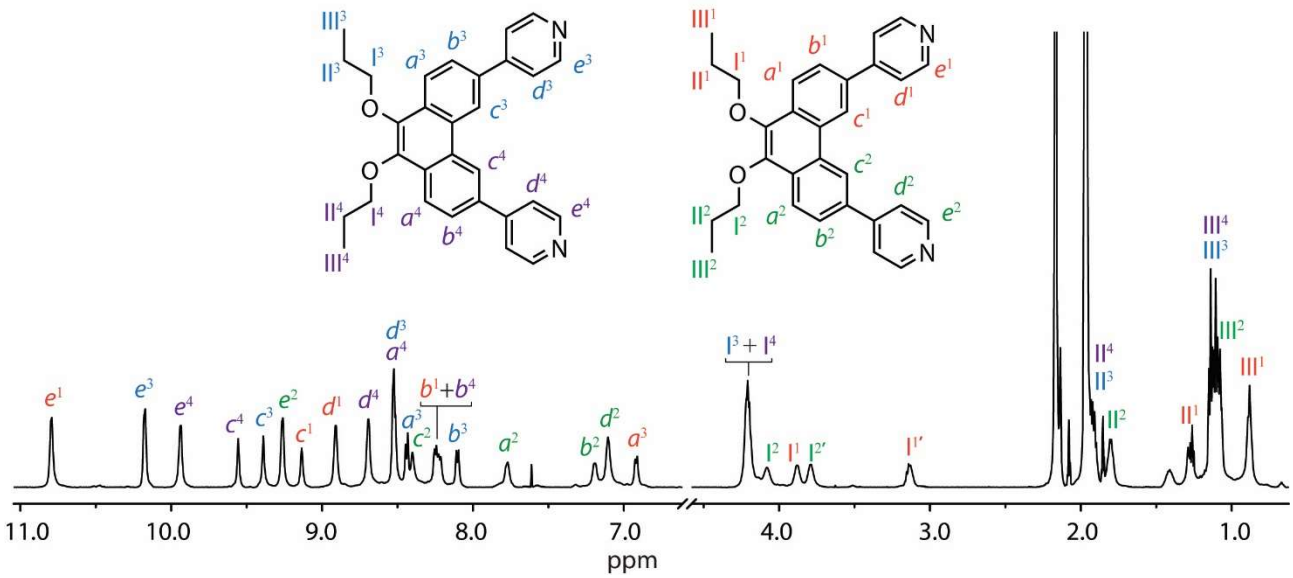

Figure S18. Partial ^{1}H NMR spectrum (600 MHz/CD_3CN) of **2b**.

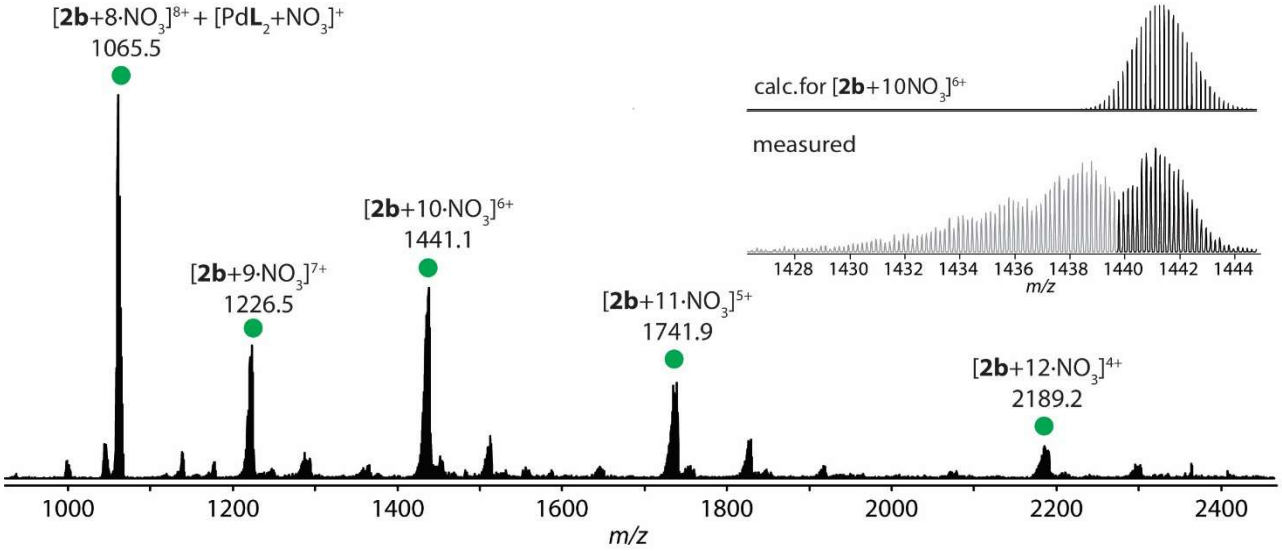

Figure S19. ESI-MS spectrum of $[Pd_8\mathbf{L^2}_{16}+n\mathrm{NO_3}]^{16-n+}$ with n = 8–12 (**2b**). The measured and calculated isotope patter of **2b**+10·NO_3 shown in the inset. Each peak contains additional overlapping peaks corresponding closely to ions of **2b** with partial cleavages of the alkyl chains.

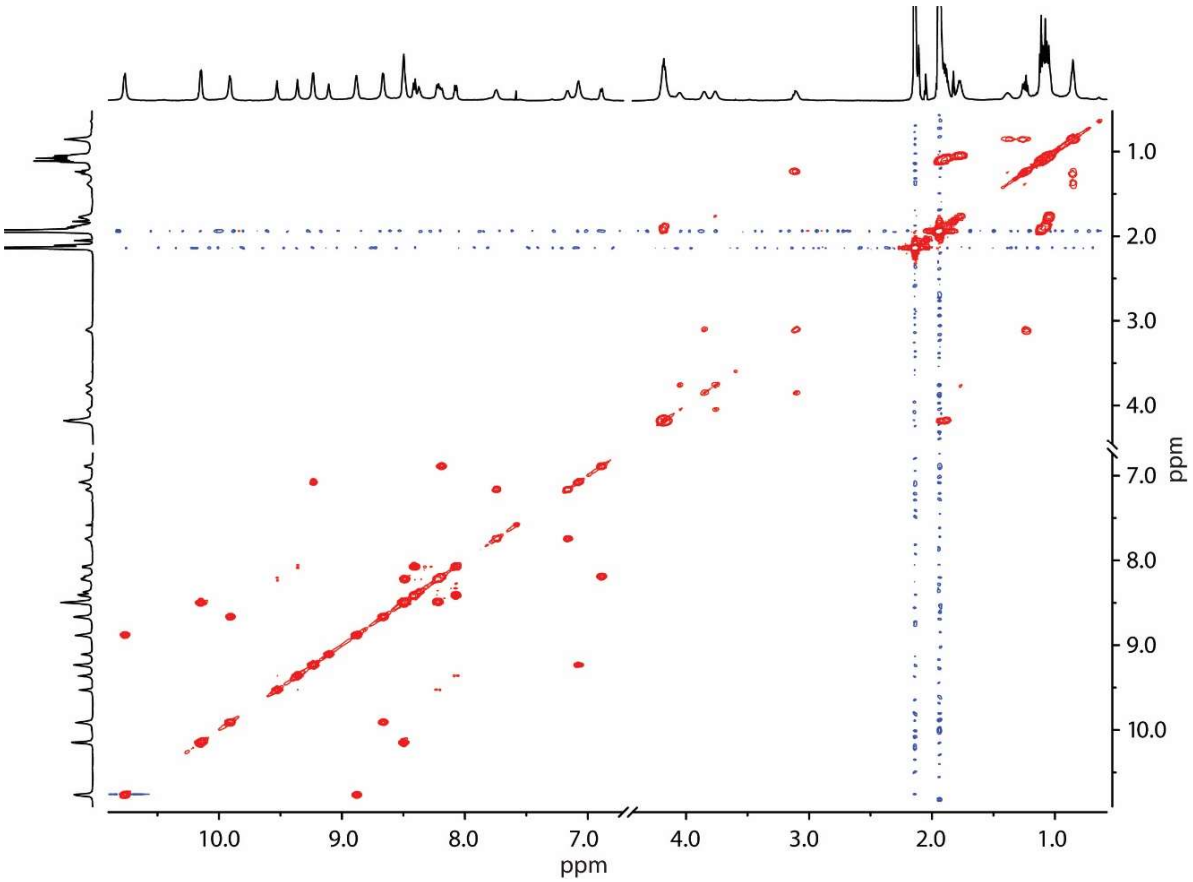

Figure S20. $^{1}H - {}^{1}H$ COSY spectrum (600 MHz/CD_3CN) of **2b**.

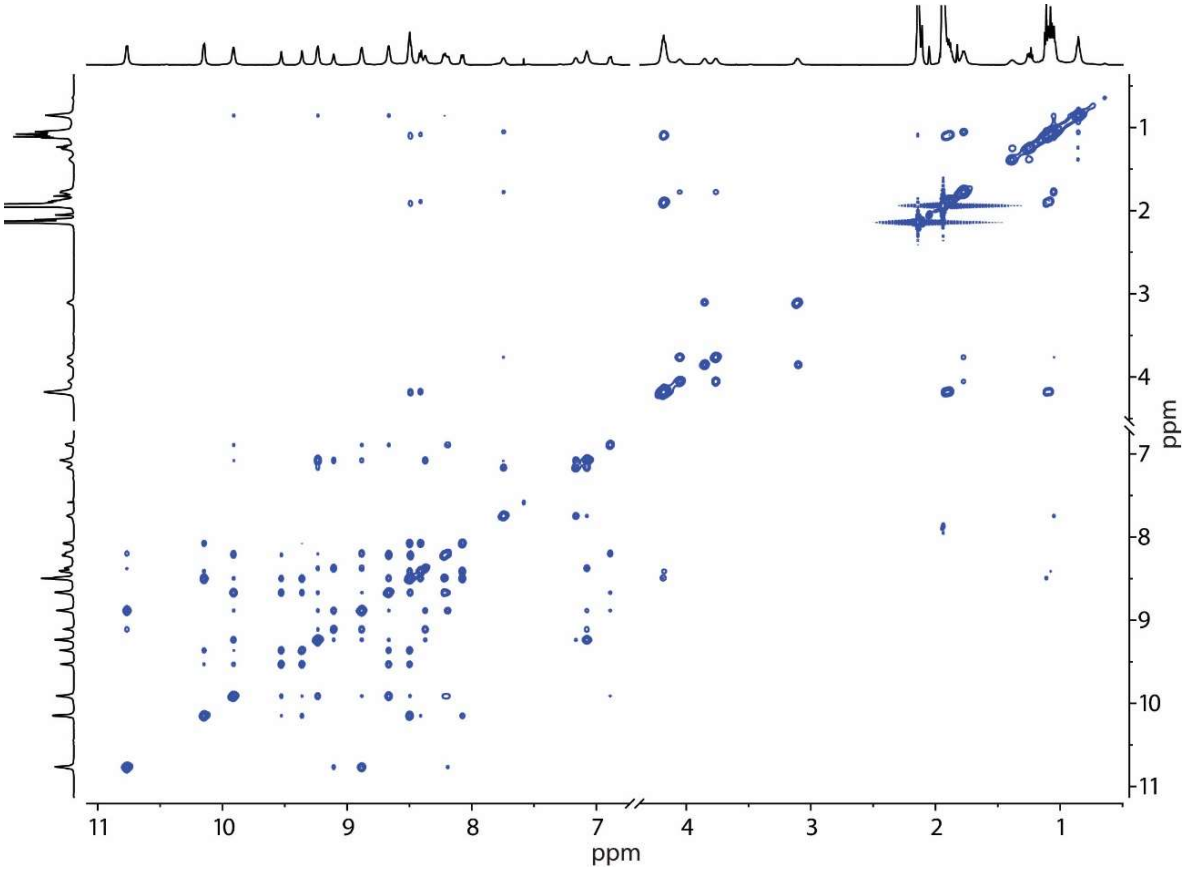

Figure S21. $^{1}H - {}^{1}H$ NOESY spectrum (600 MHz/CD_3CN) of **2b**.

*1.4.5. Synthesis of $[Pd_8\mathbf{L^3}_{16}]^{16+}$ (**2c**)*

A solution of $Pd(NO_3)_2$ (312 µL, 15 mM/CD_3CN, 4.7 µmol) was combined with a solution of $\mathbf{L^3}$ (4.84 mg, 9.1 µmol) in CD_3CN (2933 µL) and heated at 70 °C for 24 h to afford $[Pd_8\mathbf{L^3}_{16}]^{16+}$. Upon cooling to room temperature, the solution of **2c** was observed to become cloudy (Figure S33). ^{1}H NMR (500 MHz, CD_3CN, 65 °C) δ 10.76 (d, *J* = 6.2 Hz, 16H), 10.14 (d, *J* = 6.1 Hz, 16H), 9.88 (d, *J* = 6.0 Hz, 16H), 9.54 (s, 8H), 9.38 (s, 8H), 9.24 (d, *J* = 6.0 Hz, 16H), 9.10 (s, 8H), 8.87 (d, *J* = 6.1 Hz, 16H), 8.64 (d, *J* = 6.0 Hz, 16H), 8.53 – 8.46 (m, 24H), 8.44 – 8.37 (m, 16H), 8.21 (dd, *J* = 13.7, 8.7 Hz, 16H), 8.08 (d, *J* = 8.9 Hz, 8H), 7.77 (d, *J* = 8.5 Hz, 8H), 7.18 (d, *J* = 8.7 Hz, 8H), 7.11 (d, *J* = 5.9 Hz, 16H), 6.94 (d, *J* = 8.6 Hz, 8H), 4.32 – 4.18 (m, 32H), 4.16 – 4.05 (m, 8H), 3.95 – 3.73 (m, 16H), 3.30 – 3.07 (m, 8H), 1.63 – 1.49 (m, 48H), 1.47 – 1.23 (m, 208H), 0.98 – 0.84 (m, 96H). ESI HR-MS ($C_{576}H_{640}N_{32}O_{32}Pd_8$) calc: 1089.7898 [**2c**+7NO_3]$^{9+}$, 1233.7620 [**2c**+8NO_3]$^{8+}$, 1418.8692 [**2c**+9NO_3]$^{7+}$, 1665.6788 [**2c**+10NO_3]$^{6+}$; found: 1089.7793 [**2c**+7NO_3]$^{9+}$,1233.7542 [**2c**+8NO_3]$^{8+}$, 1418.8607 [**2c**+9NO_3]$^{7+}$, 1665.6679 [**2c**+10NO_3]$^{6+}$.

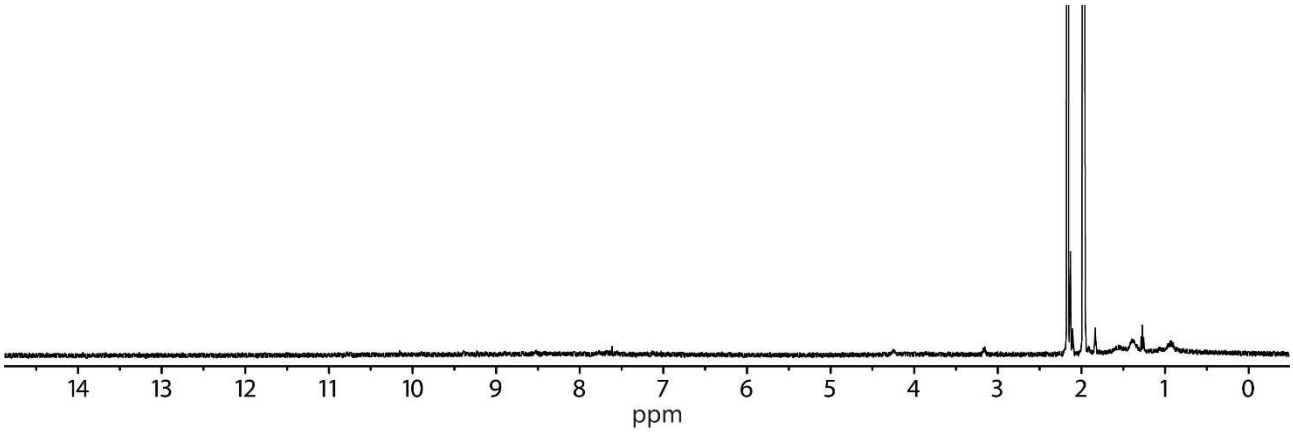

Figure S22. ^{1}H NMR spectrum (500 MHz/CD_3CN, 25 °C) of **2c.**

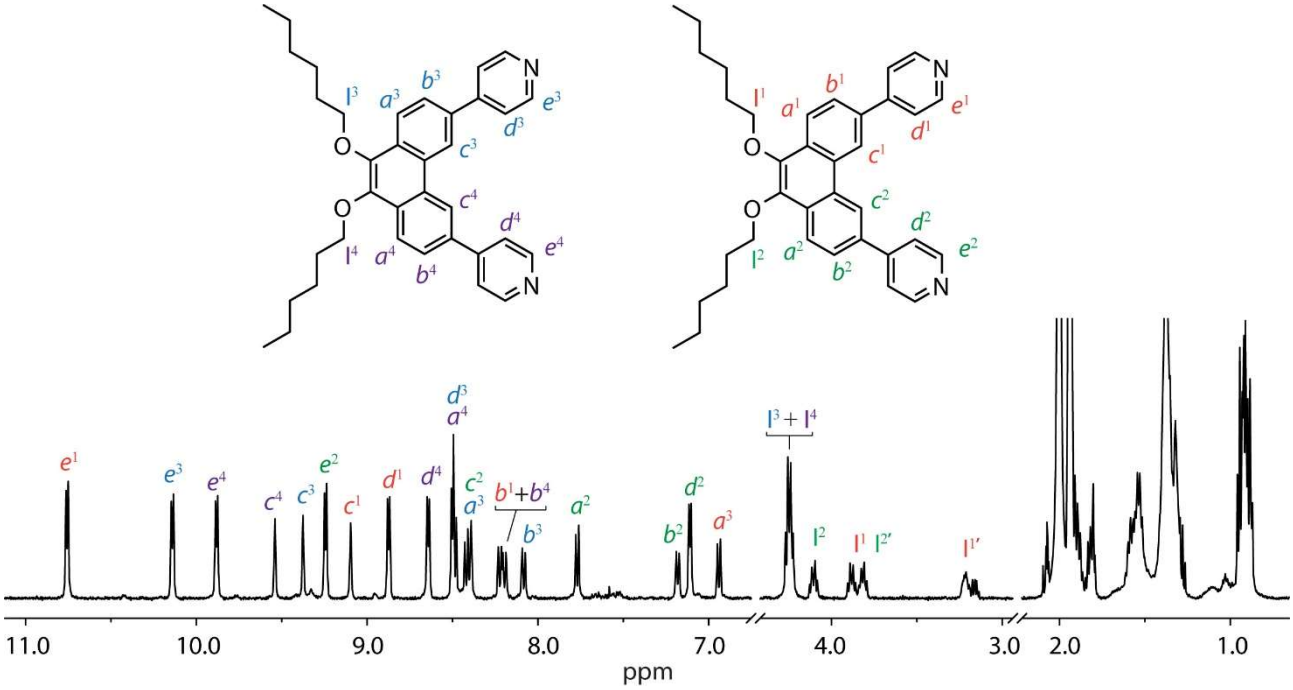

Figure S23. Partial ^{1}H NMR spectrum (600 MHz/CD_3CN, 65 °C) of **2c.**

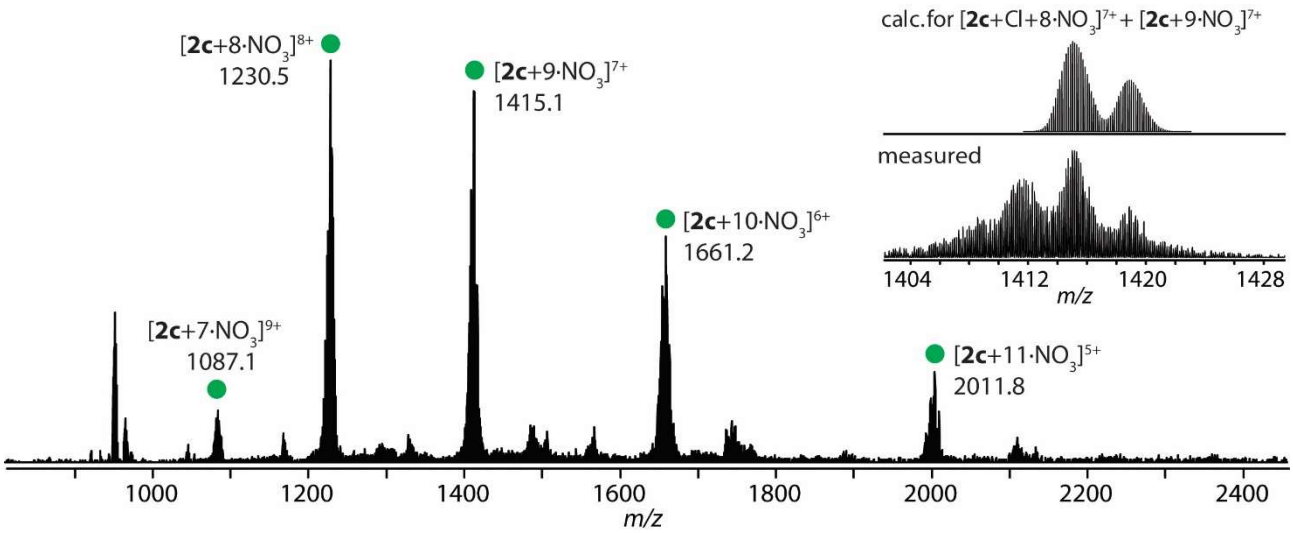

Figure S24. ESI-MS spectrum of $[Pd_8\mathbf{L^3}_{16}+n NO_3]^{16-n+}$ with n = 7–11 (**2c**) with the measured and calculated isotope patter of $[\mathbf{2c}+9\cdot NO_3]^{7+}$ / $[\mathbf{2c}+Cl+8\cdot NO_3]^{7+}$ shown in the inset. Each peak contains additional species of **2c** with masses corresponding closely to the partial cleavages of the alkyl chain. 20% DMSO was added to disrupt the aggregation of **2c** for the measurement.

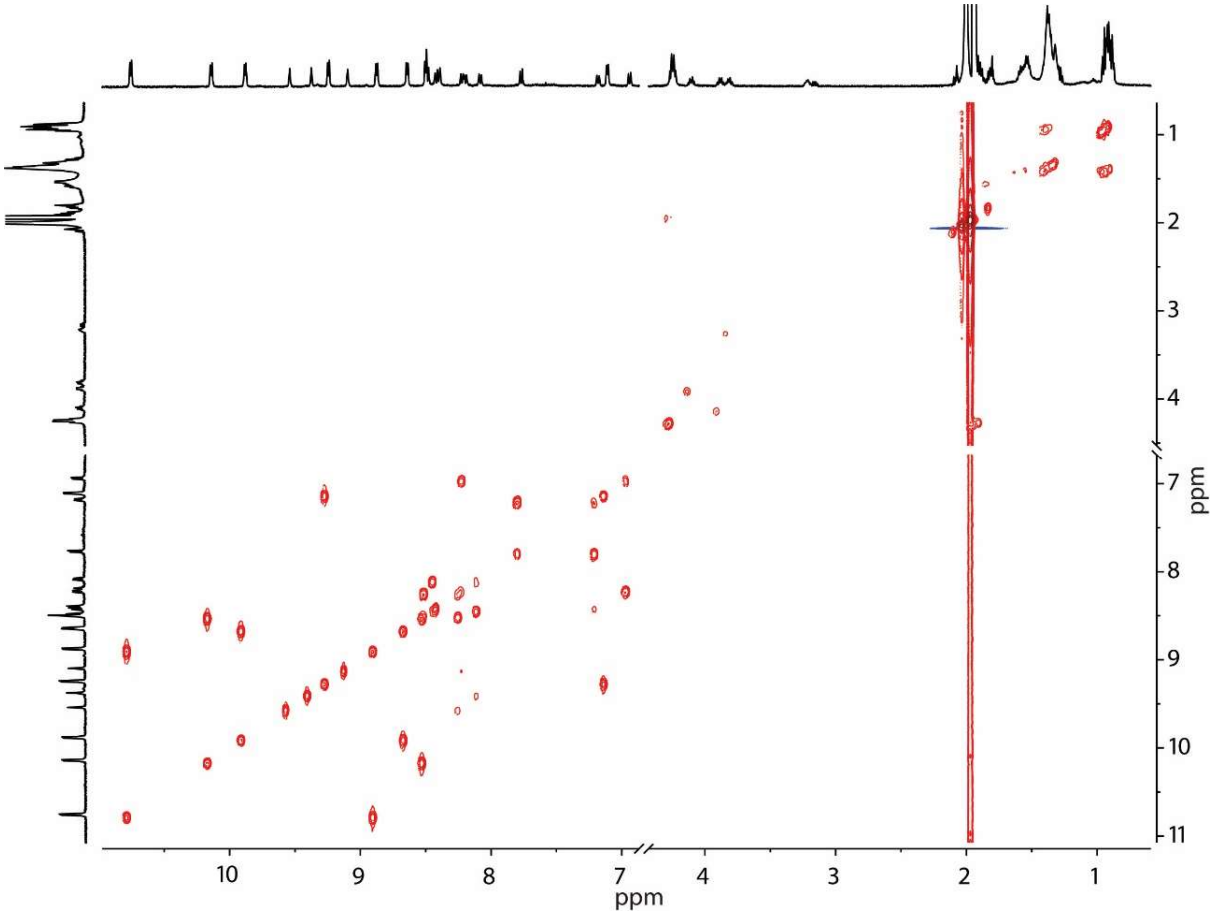

Figure S25. ^1H – ^1H COSY spectrum (600 MHz/CD_3CN) of **2c**.

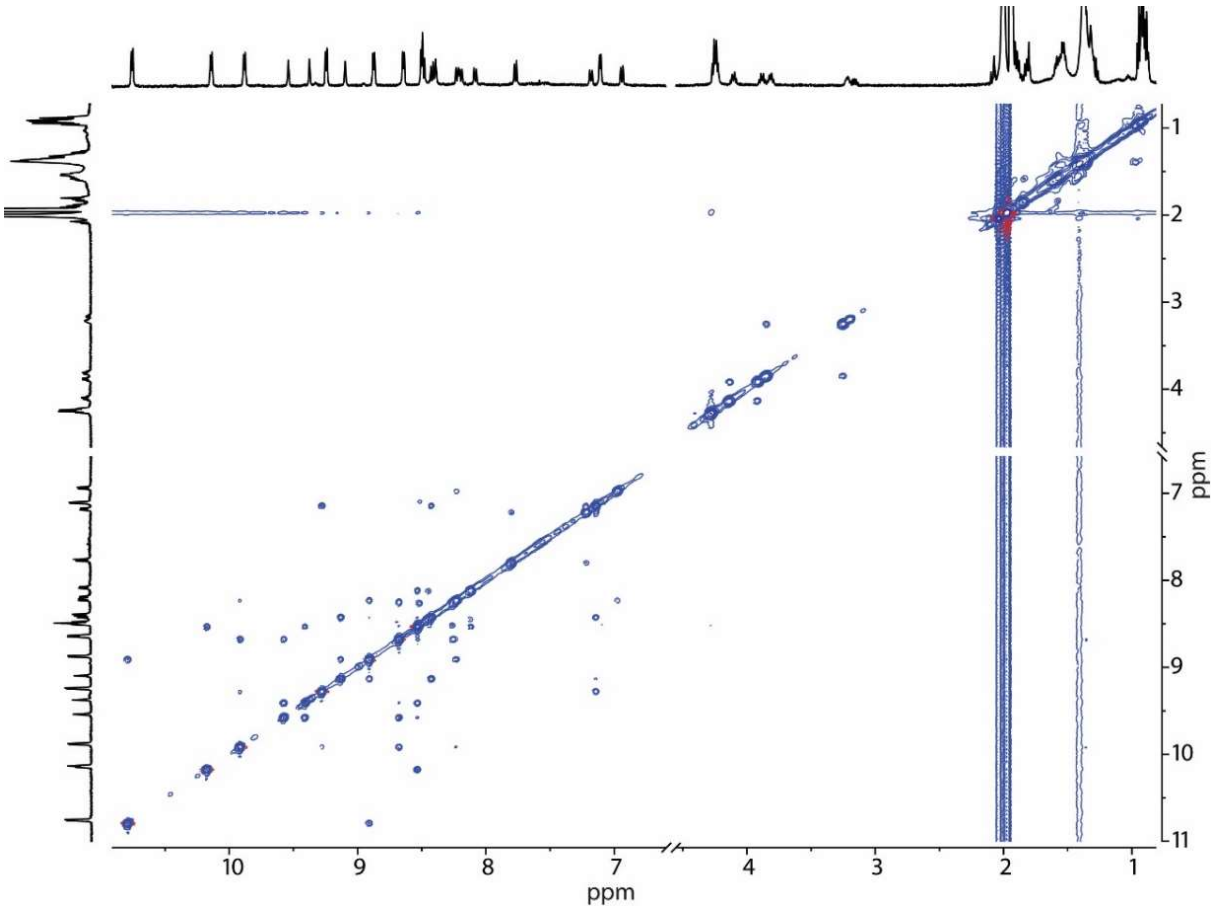

Figure S26. ^{1}H – ^{1}H NOESY spectrum (600 MHz/CD_3CN) of **2c**.

2. NO_3^- triggered transformation

Tetrabutylammonium nitrate (TBA NO_3) in CD_3CN (4, 8 or 12 equivalents, 17.5 mM solution) was added to the mixture of $[Pd_3\mathbf{L^1}_6](BF_4)_6$, $[Pd_4\mathbf{L^1}_8](BF_4)_8$ (D_{4h}), and $[Pd_4\mathbf{L^1}_8](BF_4)_8$ (D_{2d}) (**1a**, **1b** and **1c**) in CD_3CN. The mixture was heated at 70 °C for 24 h and ^{1}H NMR spectra of the reaction mixture were recorded (below). For the ^{15}N labelled experiment, TBA $^{15}NO_3$ was prepared from commercially available $K^{15}NO_3$ (98% ^{15}N labelled). A 17.5 mM stock solution (9:1 CD_3CN/D_2O) was made up by dissolving $K^{15}NO_3$ in D_2O and subsequently adding TBA Cl in CD_3CN. A precipitate was observed (KCl) after 10 seconds and the mixture was heated at 70 °C for 3 h. After filtering off the precipitate the solution of TBA $^{15}NO_3$ was obtained.

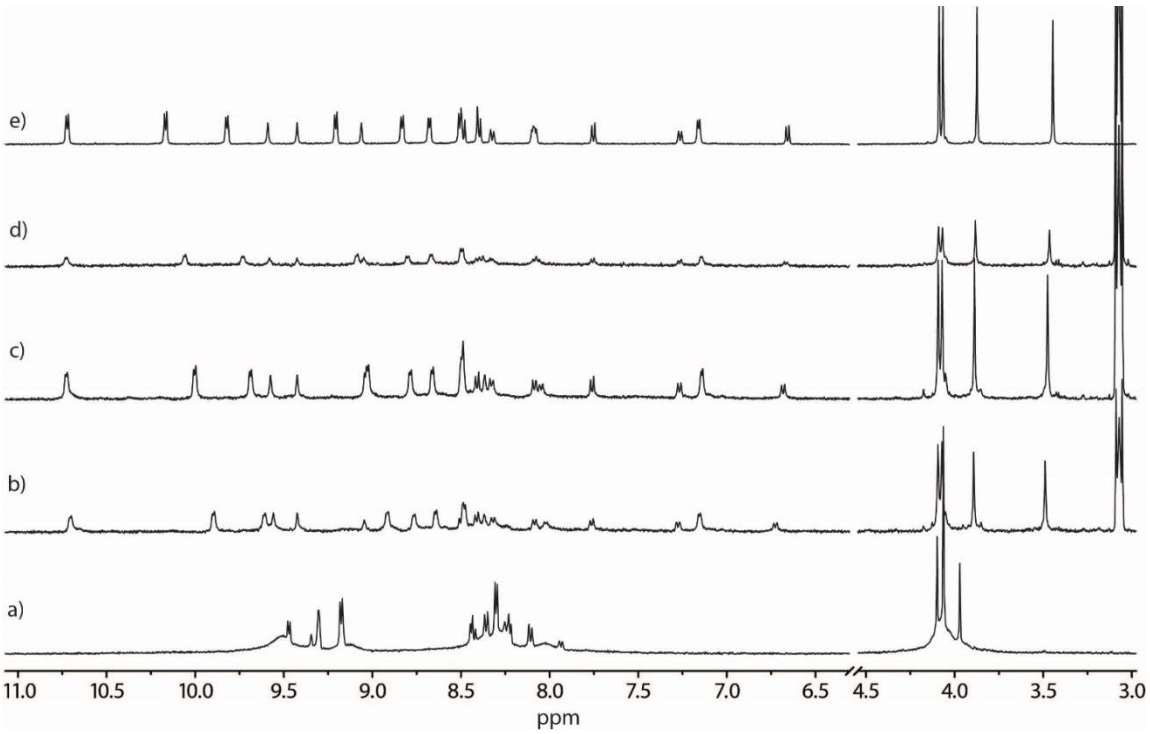

Figure S27. ^{1}H NMR spectrum (500 MHz/CD_3CN) of: a) The mixture of **1a**/**1b**/**1c** obtained by heating **L¹** with $[Pd(CH_3CN)_4](BF_4)_2$ for 2 h at 70 °C ; b) a) with 4 equiv. of NO_3^-, after heating for 24 h; c) a) with 8 equiv. of NO_3^-, after heating for 24 h; d) a) with 12 equiv. of NO_3^-, after heating for 24 h; e) **2a** obtained directly from $Pd(NO_3)_2$. Note: the best conversion of **1a**/**1b**/**1c** to **2a** occurs with 8 equiv. of NO_3^- (spectrum shown in c)). Relative to c) the yield of **2a** in b) and d) is 54 %, 33% respectively (calculated by comparing the average ratio of 4 aromatic protons of **2a** to the TBA cation signal at 3.07 ppm). The lower yield of **2a** in b) is presumably due to a minimum amount of NO_3^- anions required for the formation of the structure. In c) however, addition of more than 8 equivalents of NO_3^- results in the immediate formation of some precipitate. The small discrepancies in the shifts of the aromatic protons between b) – e) is presumably due to fast exchange of the BF_4^- anions at the periphery of the structure.

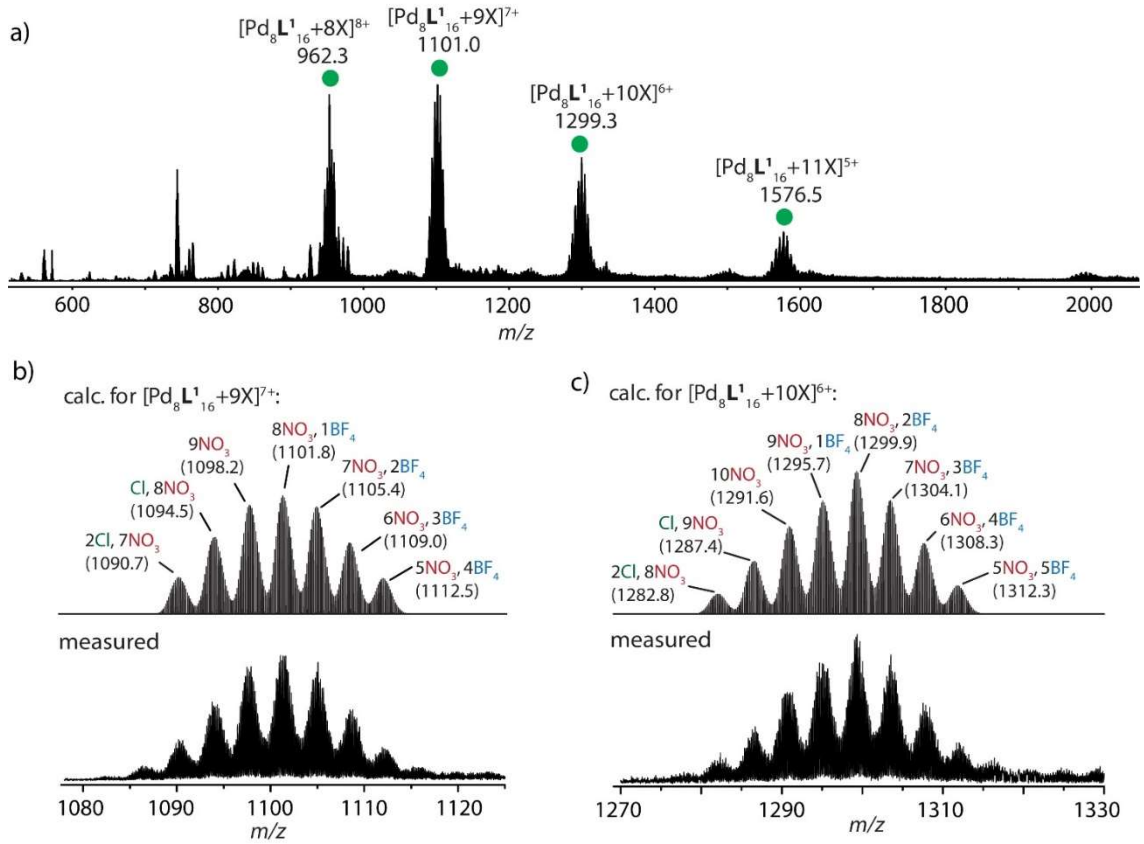

Figure S28. a) ESI-MS spectrum of a mixture of **1a**, **1b**, and **1c** (counter-ion BF_4^-) after heating with 8 equiv. tetrabutylammonium nitrate at 70 °C for 24 h; $[Pd_8\mathbf{L^1}_{16}+nX]^{16-n+}$ with n = 8–11 (X = Cl^-, NO_3^-, BF_4^-). b) Calculated and measured isotope pattern of the 7+ peak; c) calculated and measured isotope pattern of the 6+ peak. Note: Cl^- ions are present as a contaminant.

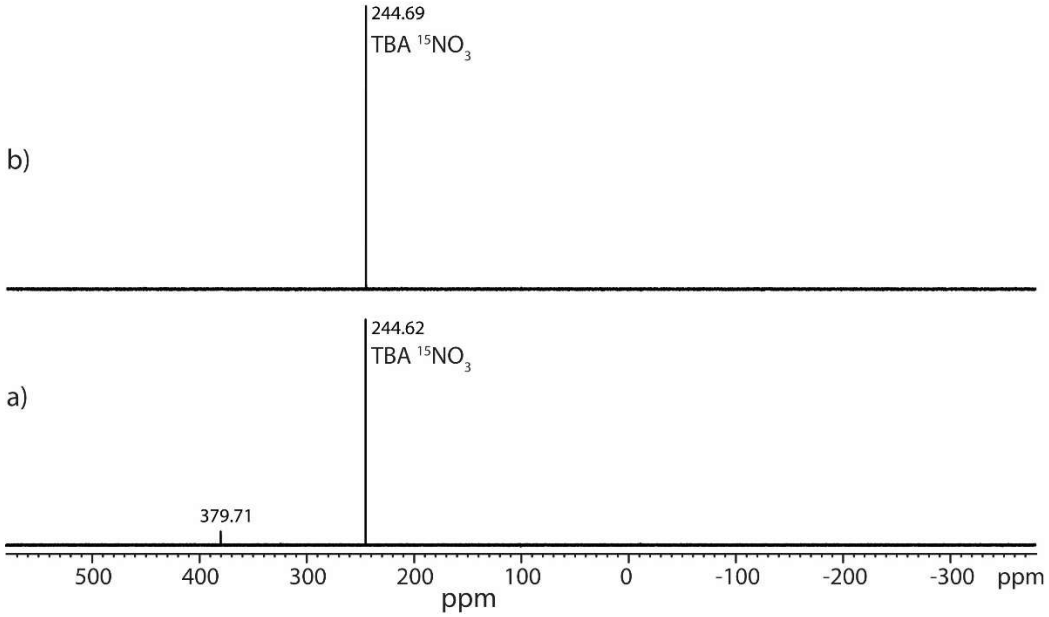

Figure S29. ^{15}N NMR spectra (60.827 MHz/CD_3CN) measured on an AVANCE-III HD 600 equipped with a BBFO cryo-probe; a) TBA $^{15}NO_3$ (244.62 ppm). The signal at 379.71 ppm is presumed to be unreacted $K^{15}NO_3$; b) **2a** obtained by heating he mixture of **1a**/**1b**/**1c** with 8 equiv. of TBA $^{15}NO_3$ for 24 h at 70°C.

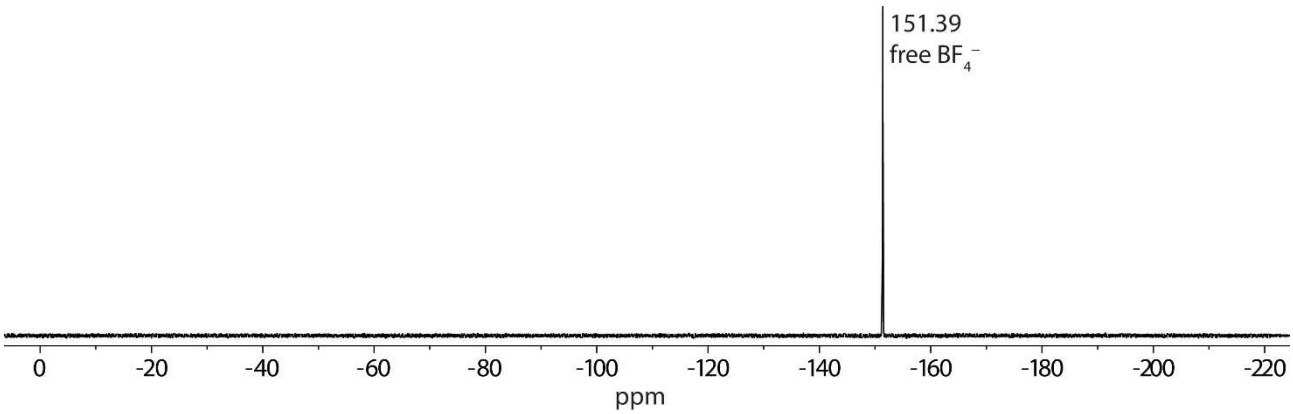

Figure S30. ^{19}F NMR spectra (377 MHz/CD_3CN) of **2a** obtained by heating he mixture of **1a**/**1b**/**1c** with 8 equiv. of TBA $^{15}NO_3$ for 24 h at 70°C.

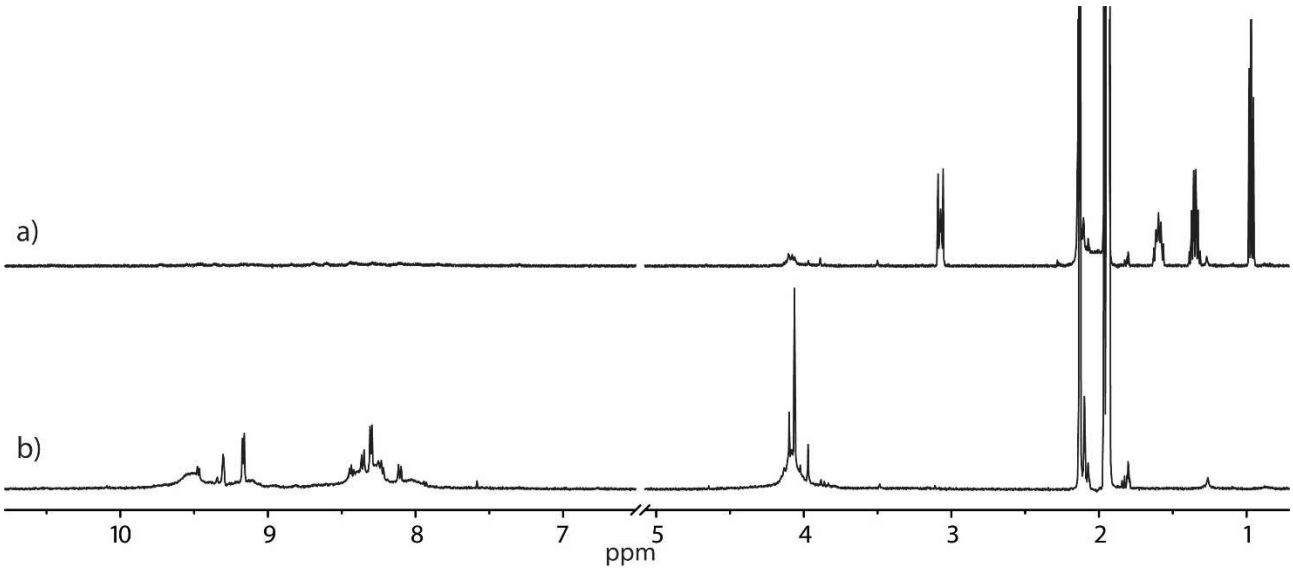

Figure S31. ^{1}H NMR spectrum (500 MHz, CD_3CN) of; a) The mixture of **1a**/**1b**/**1c** obtained by heating **L^1** with $[Pd(CH_3CN)_4](BF_4)_2$ for 2 h at 70 °C; b) the same mixture after heating for 24 h at 70 °C in the presence of 8 equiv. of PF_6^-.

3. Dynamic light scattering (DLS)

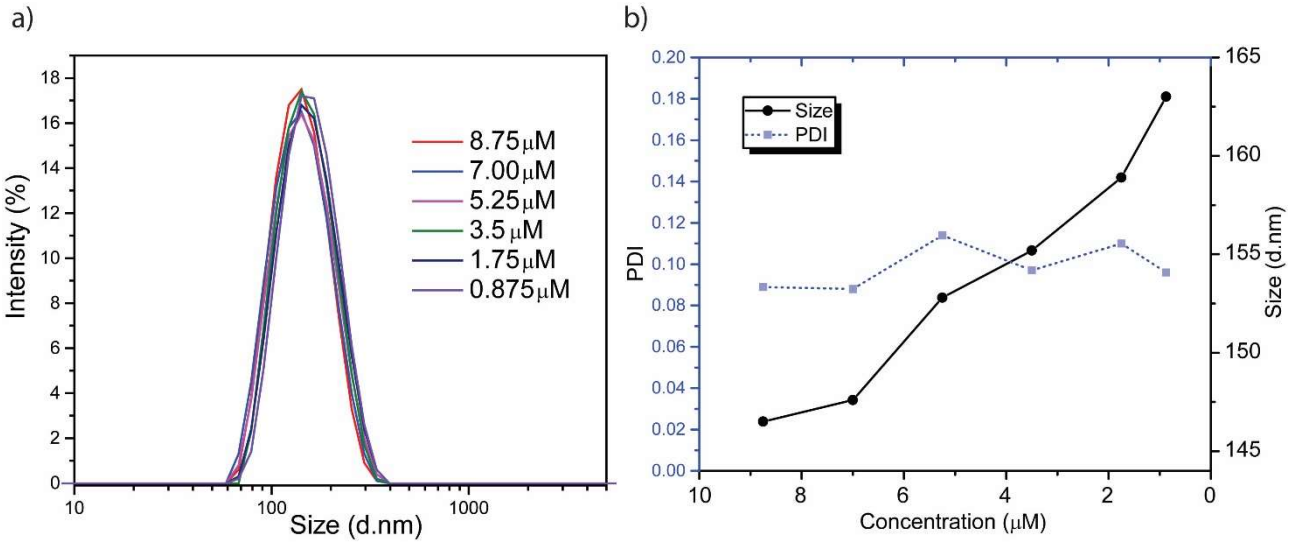

Figure S32. DLS of **2c** measured at different concentrations; a) intensity distribution overlay; b) plot of hydrodynamic diameter (d.nm) versus concentration with PDI shown (light blue) for each measurement. Note: each measurement is an average of three measurements. The vesicle-like particles of **2c** show an inverse concentration dependent swelling.

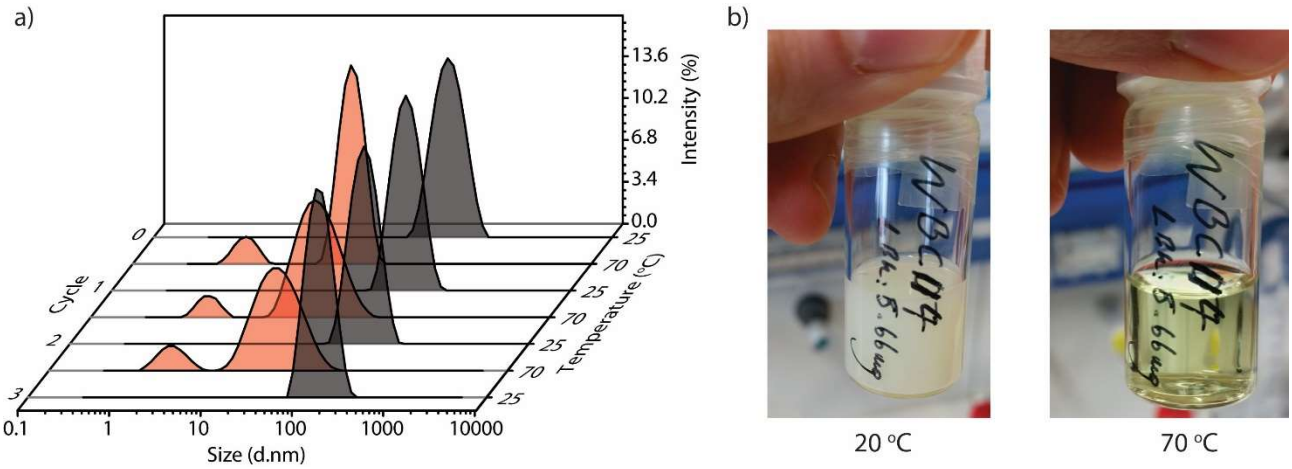

Figure S33. a) DLS of **2c** cycled between 25 and 70 °C. Upon heating (red), a smaller aggregate is observed (36.2 ± 20.4 nm) along with particles measuring 2.3 ± 0.7 nm (corresponding to non-aggregated **2c**). Upon cooling (grey), the original aggregate (157.6 ± 44.9 nm) is recovered. Concentration of **2c** = 5.25 μM; b) a picture of **2c** in MeCN at room temperature (left) and at 70 °C (right).

4. Transmission electron microscopy (TEM)

Samples of **2a** and **2c** were prepared in CH_3CN (0.0875 mM) and deposited on a copper electron microscopy grid. The solvent was allowed to evaporate and then the sample was put under vacuum for 30 minutes prior to immediate measurement.

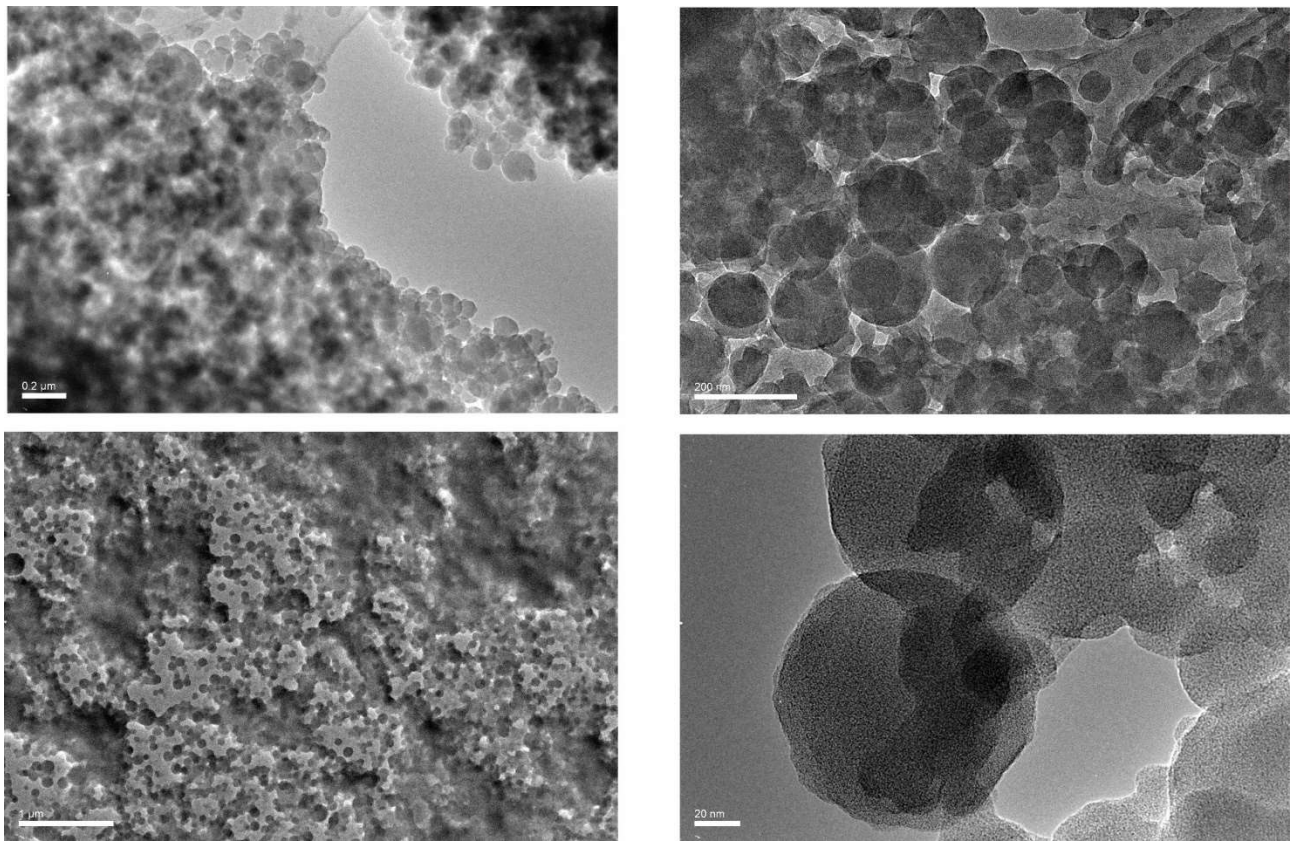

Figure S34. TEM images of **2c** at different magnifications.

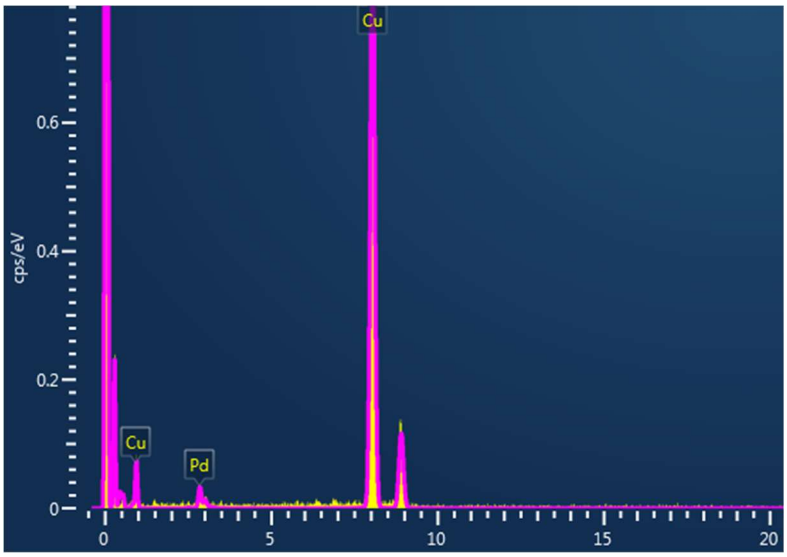

Figure S35. An example of a raw EDX spectrum of **2c**, confirming the palladium composition of the sample visualized by TEM.

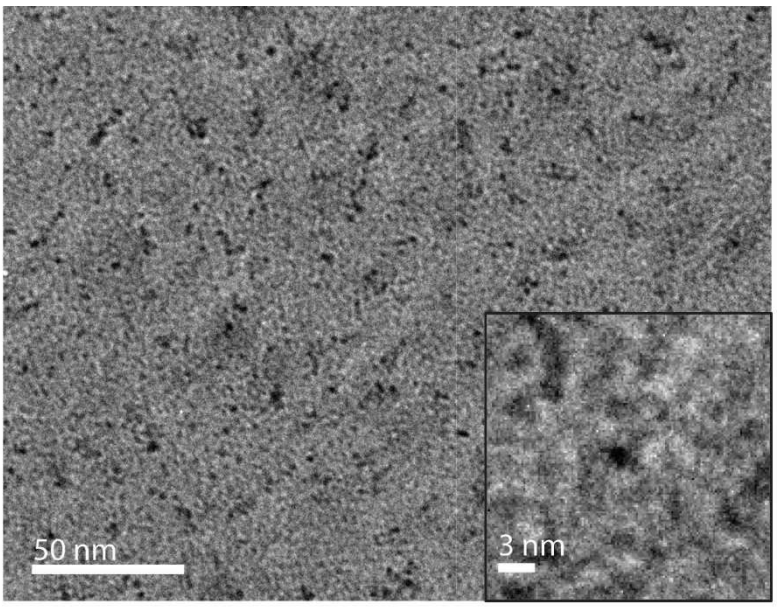

Figure S36. TEM image of **2a**. The dark circles measure 2 – 3 nm is diameter, which compares well to the diameter of **2a** in solution (D_H = 2.48 Å) and the solid-state (2.5 Å – longest dimensions of the cigar-shaped structure).

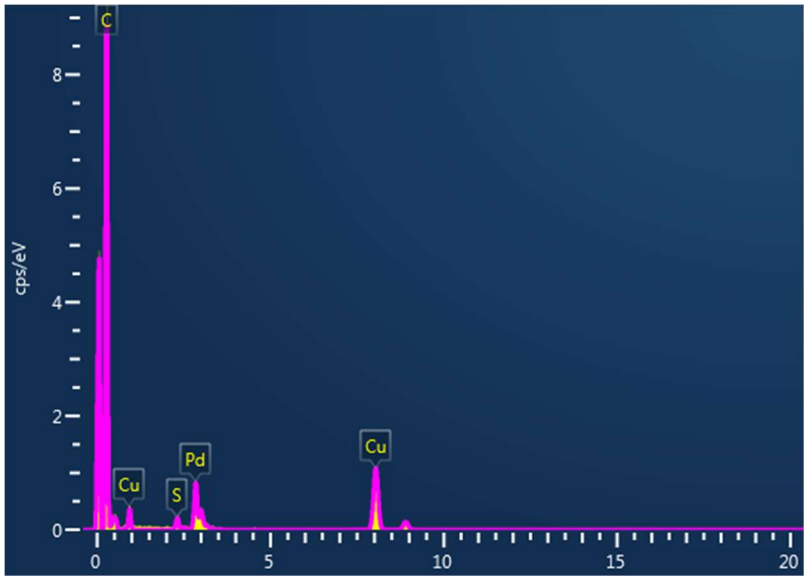

Figure S37. An example of a raw EDX spectrum of **2a**, confirming the palladium composition of the sample visualized by TEM.

5. Formation of D_{2d}-[Pd$_4$L$^1_8$] (1c)

5.1. DFT calculations

All models were constructed using SPARTAN[6] and were first optimized with the PM6 semi-empirical method. The resulting structures were then further refined by DFT calculations carried out with GAUSSIAN.[7]

As discussed here and elsewhere,[5] when **L^1** is reacted with [Pd(CH$_3$CN)$_4$](BF$_4$)$_2$, D_{2d}-[Pd$_4$**L$^1_8$**] (**1c**) forms only as the minor product along with major products D_{4h}-[Pd$_4$**L$^1_8$**] (**1b**) and D_{3h}-[Pd$_3$**L$^1_6$**] (**1a**). We performed DFT calculations to provide insight into why **1c** might be less stable than its structural isomer **1a**. Indeed, DFT calculations (RB3LYP, def2/svp) revealed that **1c** is 35.4 kcal/mol higher is energy than **1a**, presumably due to the bond strain in one of the two bridging modes of **L^1**.

Level of theory: B3LYP/def2-SVP. D_{4h} box: E(hartree): -10604.3416736, D_{2d} tetrahedron: -10604.2852263

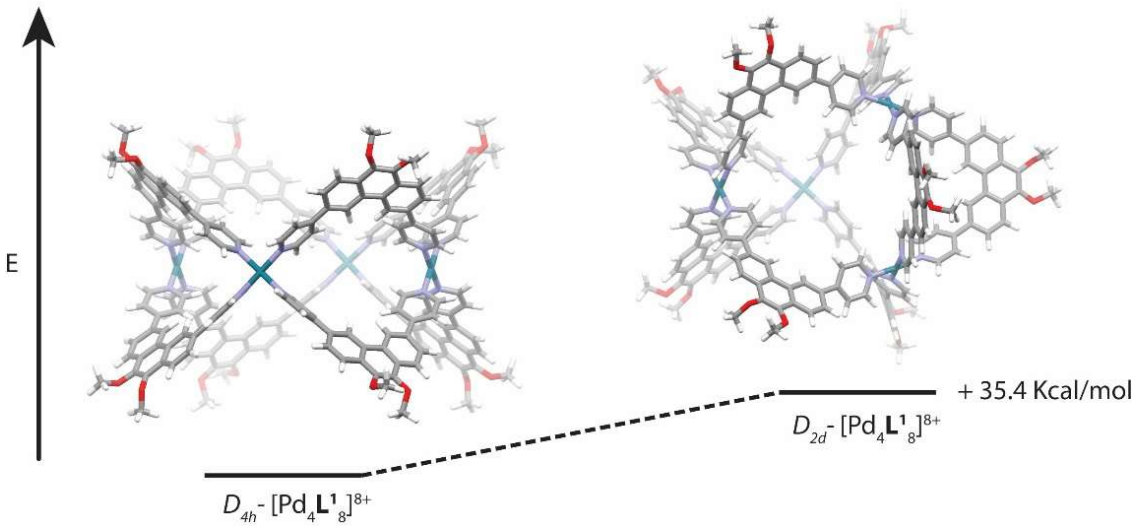

Figure S38. DFT calculated structures and relative energies for D_{4h}-[Pd_4**L**$^1{}_8$]$^{8+}$ and D_{2d}-[Pd_4**L**$^1{}_8$]$^{8+}$ (**1b** and **1c** respectively).

5.2. Discussion

We were surprised when a single crystal of **1c** was isolated after slow vapour diffusion of THF into a solution of [Pd_8**L**$^1{}_{16}$] (**2a**) in MeCN. It is important to note that the crystallization occurred over a period of 3 months, and only three small (0.1 mm^3) crystals were observed on the walls of the vial. Therefore, only a very small amount of the material crystallized with the remaining material observed in the form of a precipitate. An explanation for this could be that, after the initial precipitation, significant dilution of the **2a** by slow diffusion of THF shifts the equilibrium toward non-interpenetrated products. One would therefore expect **1b** to be the major product (as it is the non-interpenetrated monomeric form of **2a**). An explanation for this could be that the presence of NO_3^- anions stabilizes **1c**, or that **1c** packs more favourably in the solid-state than **1a** or **1b**. To test the former hypothesis, we titrated the mixture of **1a**/**1b**/**1c** with TBA NO_3^- and allowed the mixture to equilibrate over 3 days before measuring the ^{1}H NMR spectrum. As can be seen from the figure below, addition of NO_3^- anions does indeed shift the equilibrium towards **1c** as the major product.

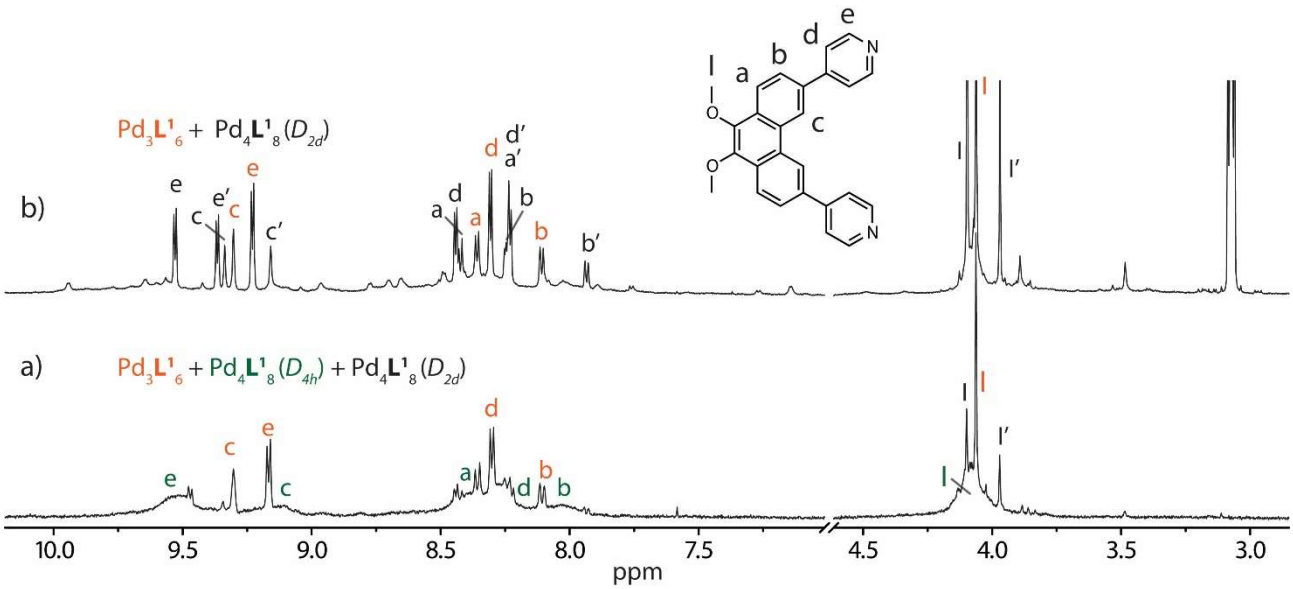

Figure S39. ^{1}H NMR spectra (500 MHz/CD_3CN) of: a) a mixture of **1a**, **1b** and **1c** (approximate ratio: 1:2:0.2, respectively); b) the same sample with 1 equivalent of TBA NO_3^- after 3 days at 25 °C. Ratio of **1a** to **1c**: 3:4. **1b** (D_{4h}-[Pd_4**L**$^1{}_8$]) could not be detected.

6. X-ray crystallography

Compound	**1c**	**2b**
CCDC number	1811308	1811309
Empirical formula	$C_{216}H_{176}N_{20}O_{30}Pd_4$	$C_{480}H_{448}N_{44}O_{68}Pd_8$
Formula weight	3957.36	4386.00
Temperature (K)	100(2)	80(2)
Crystal system	Tetragonal	Monoclinic
Space group	P-4n2	$P2_1/n$
a (Å)	24.778(4)	25.489(5)
b (Å)	24.778(4)	93.914(19)
c (Å)	22.718(5)	26.030(5)
α (°)	90	90°
β (°)	90	93.00(3)°
γ (°)	90	90°
Volume ($Å^3$)	13948(5)	62225(22)
Z	2	4
Density (calc.) (Mg/m^3)	0.942	0.936
Absorption coefficient (mm^{-1})	0.751	0.256
F(000)	4072	18192
Crystal size (mm^3)	0.100 x 0.050 x 0.010	0.200 x 0.200 x 0.100
θ range for data collection (°)	1.635 to 28.209	0.420 to 15.608
Reflections collected	63660	205892
Observed reflections [R(int)]	6103 [0.0333]	31034 [0.0323]
Goodness-of-fit on F^2	1.168	2.647
R_1 [I>2σ(I)]	0.0591	0.1809
wR_2 (all data)	0.1940	0.5315
Largest diff. peak and hole (e.Å-3)	0.440 and -0.223	0.947 and -0.459
Data / restraints / parameters	6103 / 1212 / 609	31034 / 17932 / 5401

6.1. Crystal structure of 1c

Single crystals of **1c** were grown over a period of 3 months by slow vapour diffusion of THF into a 0.175 mM CD_3CN solution of **2a**. A single crystal of **1c** in mother liquor was pipetted onto a glass slide containing NVH oil. To avoid collapse of the crystal lattice, the crystal was quickly mounted onto a 0.1 mm nylon loop and immediately flash cooled in liquid nitrogen. Crystals were stored at cryogenic temperature in dry shippers, in which they were safely transported to macromolecular beamline PXII at the Swiss Light Source (SLS), Paul Scherrer Institute, Villigen, Switzerland. A wavelength of λ = 0.9994 Å was chosen using a liquid N_2 cooled double crystal monochromator. Single crystal X-ray diffraction data was collected at 100(2) K on a single axis goniometer, equipped with an Oxford Cryostream 800 a Pilatus 6M. 3600 diffraction images were collected in a 360° φ sweep at a detector distance of 165 mm, 100% filter transmission, 0.1° step width and 1 second exposure time per image. The data were integrated with XDS.[8]

The structure was solved by intrinsic phasing/direct methods using SHELXT[9] and refined with SHELXL[10] using 22 cpu cores for full-matrix least-squares routines on F^2 and ShelXle[11] as a graphical user interface and the DSR program plugin was employed for modelling.[12]

*6.1.1. Specific refinement details of **1c**.*

Stereochemical restraints for the PMP ligands, THF solvent molecule and NO3 [NO_3^-] counter ions of the structure were generated by the GRADE program using the GRADE Web Server (http://grade.globalphasing.org) and applied in the refinement. A GRADE dictionary for SHELXL contains target values and standard deviations for 1,2-distances (DFIX) and 1,3-distances (DANG), as well as restraints for planar groups (FLAT). Due to the location of the THF on a special position (2-fold axis) the GRADE restraint dictionary was modified manually to cover symmetry generated atoms. All displacements for non-hydrogen atoms were refined anisotropically. The refinement of ADP's for carbon, nitrogen and oxygen atoms was enabled by a combination of similarity restraints (SIMU) and rigid bond restraints (RIGU).[13] The contribution of the electron density from disordered counterions and solvent molecules, which could

not be modelled with discrete atomic positions were handled using the SQUEEZE[14] routine in PLATON[15]. The solvent mask file (.fab) computed by PLATON were included in the SHELXL refinement via the ABIN instruction leaving the measured intensities untouched.

*6.1.2. Description of the structure of **1c***

1c crystallizes in the tetragonal space group P-4n2, with two molecules of **L¹**, one Pd(II) centre, one NO_3^- counter-ion and half of a THF molecule in the asymmetric unit (the other nitrate counter-ion could not be adequately modelled from the electron density in the difference map. In the structure of **1c**, four Pd atoms form an ideal tetrahedron, with the doubly-bridged Pd – $(\mathbf{L})_2$ – Pd distances (12.02 Å) being almost equal to singly bridged P – **L** – Pd connections (12.07 Å). One bridging mode of **L¹** results in an out-of-plane bending of the pyridyl donors, consistent with the bond strain predicated in the calculated model.

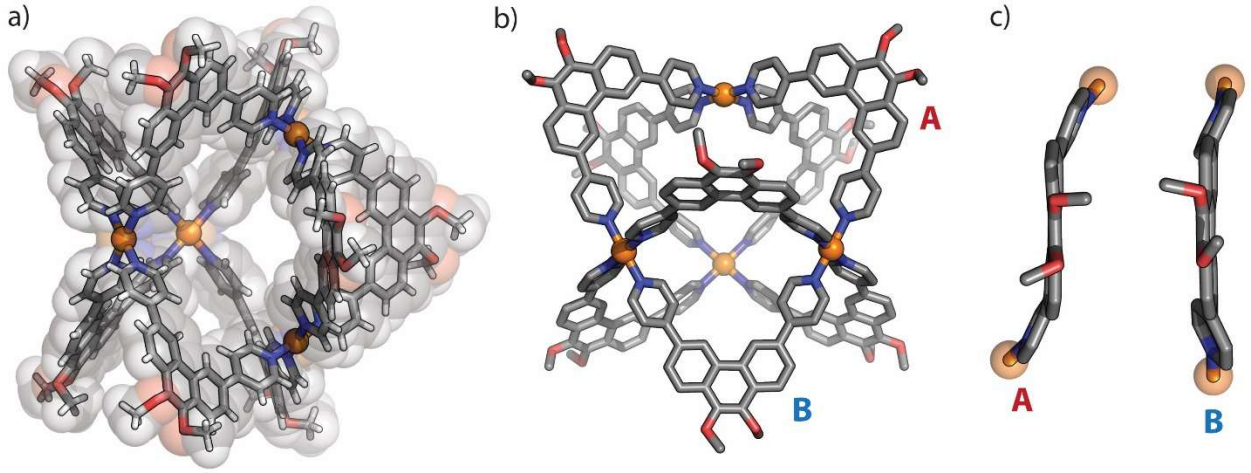

Figure S40. X-ray structure of **1c**; a) Space-filling overlay; b) perspective view with hydrogen atoms omitted for clarity; c) the two types of ligand geometries in **1c**. The pyridyl donors of ligand '**A**' are significantly twisted out of plane (with respect to the phenanthrene core) which is in accordance with the DFT calculations.

6.2. Crystal structure of 2b

Single crystals of **2b** were grown over a period of 11 days by slow vapour diffusion of diisopropyl ether into a concentrated (0.35 mM) CD_3CN solution of **2b**. A single crystal of **2b** in mother liquor was pipetted onto a glass slide containing NVH oil. To avoid collapse of the crystal lattice, the crystal was quickly mounted onto a 0.2 mm nylon loop and immediately flash cooled in liquid nitrogen.

Crystals were only poorly diffracting up to 2 Å resolution on our in-house diffractometer Bruker D8 venture equippend with an Incoatec microfocus source (Iμs 2.0) using Cuk_α radiation and 240 seconds exposure time per 1° rotation. In order to achieve a higher resolution sufficient for structure solution using direct methods (1.4 Å), an extremely bright 3rd generation source of synchrotron radiation was required. For this purpose, 20 crystals mounted on loops were placed in UNI Pucks and stored at cryogenic temperature in dry shippers, in which they were safely transported to macromolecular beamline P11[16] at Petra III, DESY, Germany. UNI Pucks were transferred to the sample dewar and all samples were mounted using the StäubliTX60L robotic arm. A wavelength of 0.6889 Å was chosen using a liquid N_2 cooled double crystal monochromator. Single crystal X-ray diffraction data was collected at 80(2) K on a single axis goniometer, equipped with an Oxford Cryostream 800 a Pilatus 6M fast. As initial screening showed significant dispersive scattering contributions and a distinct diffraction limit of approximately 1.4 - 1.3 Å, 1800 diffraction images were collected in a 360° φ sweep at a detector distance of 300 mm, 30% filter transmission, 0.2° step width and 0.2 seconds exposure time per image. Data integration and reduction were undertaken using XDS.[8] The data was cut at 1.28 Å, as the signal to noise ratio has dropped below $I/\sigma(I) < 2.0$. Due to high mosaicity, disorder in the solvent region and significant dispersive scattering contributions a higher resolution could not be achieved. The structure was solved by intrinsic phasing/direct methods using SHELXT[9] and refined with SHELXL[10] using 22 cpu cores and ShelXle[11] as a graphical user interface and the DSR program plugin was employed for modelling.[12] All modelling cycles were refined against F^2 until convergence using the conjugate-gradient algorithm (CGLS). Only for computing the crystallographic information file (CIF) the full-matrix least-squares routine was employed. Hydrogen atoms were included as invariants at geometrically estimated positions

*6.2.1. Specific refinement details of **2b***

Due to the limited resolution the data/parameter ratio is poor for a small molecule structure, but not at all critical in macromolecular structure. In order to generate a molecular model and increase robustness of the refinement we have adapted and exploited techniques commonly applied in macromolecular structure refinement. Stereochemical

restraints for the PPP ligands and NO3 [NO_3^-] counter ions of the structure were generated by the GRADE program using the GRADE Web Server (http://grade.globalphasing.org) and applied in the refinement. This macromolecular refinement technique has been adapted to be used in the program SHELXL[10] and successfully applied to other supramolecular structures behaving like macromolecules.[17–20] Also for this structure it was found to drastically increase the robustness of the refinement, especially when combined with the rigid bond restraint for atomic displacements.[13] A GRADE dictionary for SHELXL contains target values and standard deviations for 1,2-distances (DFIX) and 1,3-distances (DANG), as well as restraints for planar groups (FLAT). Non-crystallographic symmetry restraints (NCSY) were employed for 1,4-distances to enhance local structural similarity in between the 16 independent PPP ligands and thereby additionally stabilize their highly flexible propoxy side chains. All displacements for non-hydrogen atoms were refined anisotropically. The refinement of ADP's for carbon, nitrogen and oxygen atoms was enabled by a combination of similarity restraints (SIMU) and rigid bond restraints (RIGU).[13] For the NO_3^- counter ions, isotropic restraints (ISOR) were employed additionally. As the observed electron density was compelling, NO_3^- anion (residue 24) located in a pocket between two Palladium cations was modelled although the PLATON routine of CHECKCIF reported a short contacts B alert. It is possible, that there are multiple positions for this counterion, which we cannot resolve at the resolution achieved. The contribution of the electron density from disordered counterions and solvent molecules, which could not be modelled with discrete atomic positions were handled using the SQUEEZE[14] routine in PLATON.[15] The solvent mask file (.fab) computed by PLATON were included in the SHELXL refinement via the ABIN instruction leaving the measured intensities untouched.

6.3. Thermal ellipsoid plots

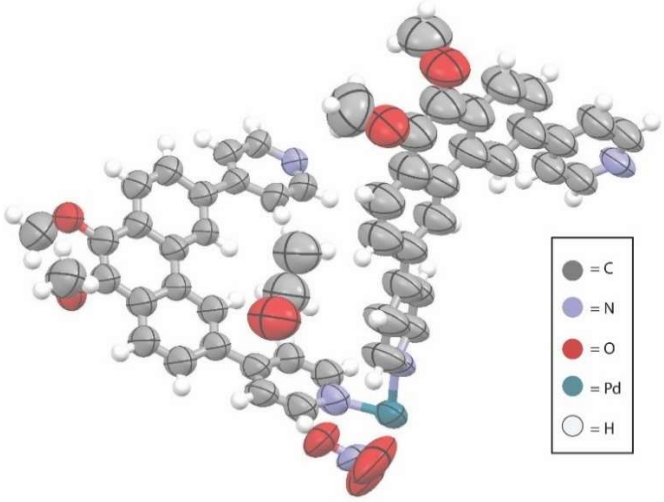

Figure S41. The asymmetric unit of the X-ray structure of **1c**, with all non-hydrogen atoms shown as ellipsoids at the 50% probability level.

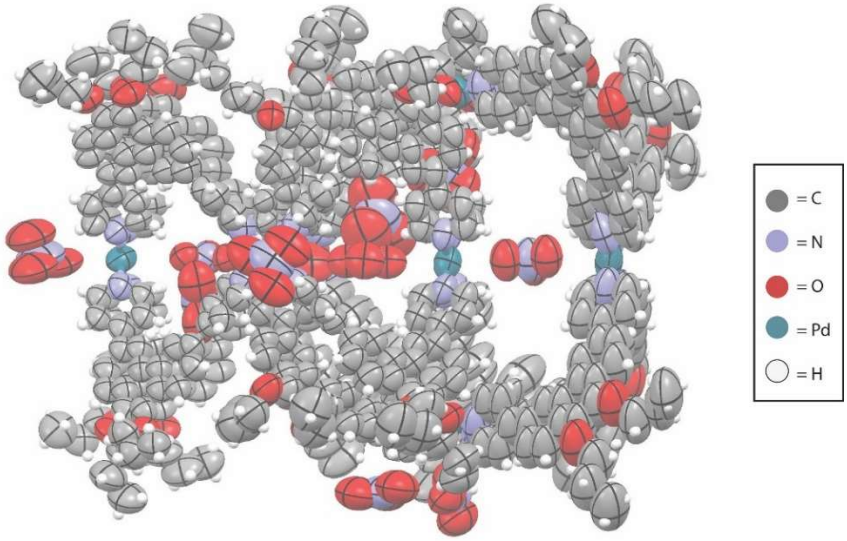

Figure S42. The asymmetric unit of the X-ray structure of **2b**, with all non-hydrogen atoms shown as ellipsoids at the 50% probability level.

7. References

1 B. N. Boden, J. K.-H. Hui and M. J. MacLachlan, *J. Org. Chem.*, 2008, **73**, 8069–8072.

2 W. M. Bloch, Y. Abe, J. J. Holstein, C. M. Wandtke, B. Dittrich and G. H. Clever, *J. Am. Chem. Soc.*, 2016, **138**, 13750–13755.

3 http://www.ddbst.com/en/EED/PCP/VIS_C3.php. [Accessed 15 November 2017].

4 B. V. Phulwale, S. K. Mishra, M. Nečas and C. Mazal, *J. Org. Chem.*, 2016, **81**, 6244–6252.

5 W. M. Bloch, J. J. Holstein, W. Hiller and G. H. Clever, *Angew. Chem. Int. Ed.*, 2017, **56**, 8285–8289.

6 Spartan '08 Version 1.2.0, Wavefunction, Inc., Irvine, CA, 2009.

7 M. J. Frisch, G. W. Trucks, H. B. Schlegel, G. E. Scuseria, M. A. Robb, J. R. Cheeseman, G. Scalmani, V. Barone, B. Mennucci, G. A. Petersson, H. Nakatsuji, M. Caricato, X. Li, H. P. Hratchian, A. F. Izmaylov, J. Bloino, G. Zheng, J. L. Sonnenberg, M. Hada, M. Ehara, K. Toyota, R. Fukuda, J. Hasegawa, M. Ishida, T. Nakajima, Y. Honda, O. Kitao, H. Nakai, T. Vreven, J. A. Montgomery Jr., J. E. Peralta, F. Ogliaro, M. J. Bearpark, J. Heyd, E. N. Brothers, K. N. Kudin, V. N. Staroverov, R. Kobayashi, J. Normand, K. Raghavachari, A. P. Rendell, J. C. Burant, S. S. Iyengar, J. Tomasi, M. Cossi, N. Rega, N. J. Millam, M. Klene, J. E. Knox, J. B. Cross, V. Bakken, C. Adamo, J. Jaramillo, R. Gomperts, R. E. Stratmann, O. Yazyev, A. J. Austin, R. Cammi, C. Pomelli, J. W. Ochterski, R. L. Martin, K. Morokuma, V. G. Zakrzewski, G. A. Voth, P. Salvador, J. J. Dannenberg, S. Dapprich, A. D. Daniels, Ö. Farkas, J. B. Foresman, J. V Ortiz, J. Cioslowski and D. J. Fox, 2009.

8 W. Kabsch, *Acta Crystallogr. Sect. D*, 2010, **66**, 125–132.

9 G. M. Sheldrick, *Acta Crystallogr. Sect. A*, 2015, **71**, 3–8.

10 G. M. Sheldrick, *Acta Crystallogr. Sect. C*, 2015, **71**, 3–8.

11 C. B. Hubschle, G. M. Sheldrick and B. Dittrich, *J. Appl. Crystallogr.*, 2011, **44**, 1281–1284.

12 D. Kratzert, J. J. Holstein and I. Krossing, *J. Appl. Crystallogr.*, 2015, **48**, 933–938.

13 A. Thorn, B. Dittrich and G. M. Sheldrick, *Acta Crystallogr. Sect. A*, 2012, **68**, 448–451.

14 A. Spek, *Acta Crystallogr. Sect. C*, 2015, **71**, 9–18.

15 A. Spek, *Acta Crystallogr. Sect. D*, 2009, **65**, 148–155.

16 A. Burkhardt, T. Pakendorf, B. Reime, J. Meyer, P. Fischer, N. Stübe, S. Panneerselvam, O. Lorbeer, K. Stachnik, M. Warmer, P. Rödig, D. Göries and A. Meents, *Eur. Phys. J. Plus*, 2016, **131**, 56.

17 G. Markiewicz, A. Jenczak, M. Kołodziejski, J. J. Holstein, J. K. M. Sanders and A. R. Stefankiewicz, *Nat. Commun.*, 2017, **8**, 15109.

18 S. P. Black, D. M. Wood, F. B. Schwarz, T. K. Ronson, J. J. Holstein, A. R. Stefankiewicz, C. A. Schalley, J. K. M. Sanders and J. R. Nitschke, *Chem. Sci.*, 2016, **7**, 2614–2620.

19 M. D. Wise, J. J. Holstein, P. Pattison, C. Besnard, E. Solari, R. Scopelliti, G. Bricogne and K. Severin, *Chem. Sci.*, 2015, **6**, 1004–1010.

20 C. S. Wood, T. K. Ronson, A. M. Belenguer, J. J. Holstein and J. R. Nitschke, *Nat. Chem.*, 2015, **7**, 354–358.